SIAM J. APPL. MATH.
Vol. 66, No. 2, pp. 648–679

IRREVERSIBLE PASSIVE ENERGY TRANSFER IN COUPLED OSCILLATORS WITH ESSENTIAL NONLINEARITY*

GAETAN KERSCHEN†, YOUNG SUP LEE‡, ALEXANDER F. VAKAKIS§, D. MICHAEL McFARLAND¶, AND LAWRENCE A. BERGMAN¶

Abstract. We study numerically and analytically the dynamics of passive energy transfer from a damped linear oscillator to an essentially nonlinear end attachment. This transfer is caused by either fundamental or subharmonic resonance capture, and in some cases is initiated by nonlinear beat phenomena. It is shown that, due to the essential nonlinearity, the end attachment is capable of passively absorbing broadband energy at both high and low frequencies, acting, in essence, as a passive broadband boundary controller. Complicated transitions in the damped dynamics can be interpreted based on the topological structure and bifurcations of the periodic solutions of the underlying undamped system. Moreover, complex resonance capture cascades are numerically encountered when we increase the number of degrees of freedom of the system. The ungrounded essentially nonlinear end attachment discussed in this work can find application in numerous practical settings, including vibration and shock isolation of structures, seismic isolation, flutter suppression, and packaging.

Key words. resonance capture, passive energy transfer, essential nonlinearity, nonlinear energy sinks, energy pumping

AMS subject classifications. 74H10, 74H15, 74H45

DOI. 10.1137/040613706

1. Introduction.

We study passive and irreversible energy transfer from a linear oscillator to an essentially nonlinear attachment, which, in essence, acts as a *nonlinear energy sink (NES)*; such energy transfer we refer to as *nonlinear energy pumping*. In previous works (Vakakis and Gendelman (2001), Vakakis et al. (2003)) grounded and relatively heavy nonlinear attachments were considered, a feature that limits their attractiveness in practical applications. To eliminate these restrictions, an ungrounded and light nonlinear attachment is considered in this work, which, in addition, possesses the feature of modularity. As shown in Lee et al. (2005), even though the system considered has a simple configuration, it possesses a very complicated structure of undamped periodic orbits, which, in turn, give rise to a complicated

*Received by the editors August 20, 2004; accepted for publication July 12, 2005; published electronically January 6, 2006. This work was funded in part by AFOSR Contract 00-AF-B/V-0813.
http://www.siam.org/journals/siap/66-2/61370.html

†Département d'Aérospatiale, Mécanique et Matériaux (ASMA), Université de Liège, B-4000 Liège, Belgium (g.kerschen@ulg.ac.be); National Technical University of Athens, P.O. Box 64042, GR-157 10 Zografos, Athens, Greece; and University of Illinois at Urbana-Champaign, 104 S. Wright St., Urbana, IL 61801. The work of this author was partially supported by grants from the Belgian National Fund for Scientific Research—FNRS, the Belgian Rotary District 1630, and the Fulbright and Duesberg Foundations, which made his visit to the National Technical University of Athens and the University of Illinois possible.

‡Department of Mechanical and Industrial Engineering, University of Illinois at Urbana-Champaign, 104 S. Wright St., Urbana, IL 61801 (yslee4@uiuc.edu).

§Corresponding author. Department of Applied Mathematical and Physical Sciences, National Technical University of Athens, P.O. Box 64042, GR-157 10 Zografos, Athens, Greece (vakakis@central.ntua.gr), and Departments of Mechanical and Industrial Engineering and of Aerospace Engineering, University of Illinois at Urbana-Champaign, 104 S. Wright St., Urbana, IL 61801 (avakakis@uiuc.edu). The work of this author was partially supported by the research grant HRAKLEITOS awarded by the Hellenic Ministry of Development (program EPEAEK II).

¶Department of Aerospace Engineering, University of Illinois at Urbana-Champaign, 104 S. Wright St., Urbana, IL 61801 (dmmcf@uiuc.edu, lbergman@uiuc.edu).

series of transitions and energy exchange phenomena in the damped dynamics. We aim to show that in this system there are at least three different mechanisms for energy pumping, based either on fundamental and subharmonic resonance captures or on nonlinear beat phenomena.

Previous works examined targeted energy transfer in systems of coupled nonlinear oscillators through energy exchanges between donor and acceptor discrete breathers due to nonlinear resonance (Kopidakis, Aubry, and Tsironis (2001), Aubry et al. (2001), Morgante et al. (2002)). In Vainchtein et al. (2004) resonant interactions between monochromatic electromagnetic waves and charged particles were studied, leading to chaotization of particles and transport in phase space. In Khusnutdinova and Pelinovsky (2003) the processes governing energy exchange between coupled Klein–Gordon oscillators were analyzed; the same weakly coupled system was studied in Maniadis, Kopidakis, and Aubry (2004), and it was shown that, under appropriate tuning, total energy transfer can be achieved for coupling above a critical threshold. In related work, localization of modes in a periodic chain with a local nonlinear disorder was analyzed (Cai, Chan, and Cheung (2000)); transfer of energy between widely spaced modes in harmonically forced beams was analytically and experimentally studied (Malatkar and Nayfeh (2003)); and a nonlinear dynamic absorber designed for a nonlinear primary was analyzed (Zhu, Zheng, and Fu (2004)).

In this work we consider the two-degree-of-freedom (DOF) system

$$\begin{aligned} &m_1\ddot{y} + k_1 y + c_1\dot{y} + c_2(\dot{y}-\dot{v}) + k_2(y-v)^3 = P(t) \\ &\qquad\Rightarrow\quad \ddot{y} + \omega_0^2 y + \lambda_1\dot{y} + \lambda_2(\dot{y}-\dot{v}) + C(y-v)^3 = F(t), \\ &m_2\ddot{v} + c_2(\dot{v}-\dot{y}) + k_2(v-y)^3 = 0 \quad\Rightarrow\quad \varepsilon\ddot{v} + \lambda_2(\dot{v}-\dot{y}) + C(v-y)^3 = 0, \end{aligned} \tag{1}$$

where $\omega_0^2 = k_1/m_1$, $C = k_2/m_1$, $\varepsilon = m_2/m_1$, $\lambda_1 = c_1/m_1$, $\lambda_2 = c_2/m_1$, and $F(t) = P(t)/m_1$. Our basic aim is to study the dynamics of irreversible energy transfer ("energy pumping") from the linear oscillator (which will be directly excited) to the nonlinear attachment (which will be assumed to be initially at rest). We show that there are at least three dynamic mechanisms that can initiate or cause such energy transfer in the damped system, and these can be studied and understood by first considering the dynamics of the underlying undamped system.

2. Review of the dynamics of the undamped system (Lee et al., 2005). Since the structure and bifurcations of the periodic orbits of the undamped and unforced system play an essential role in energy transfer phenomena in the damped and forced system, we start with a brief review of the dynamics of system (1) with $\lambda_1 = \lambda_2 = F(t) = 0$; for a more detailed discussion we refer to Lee et al. (2005).

In Figure 1 we present the various branches of periodic solutions in a frequency-energy plot. A periodic orbit is represented by a point in the plot, and a branch, represented by a solid line, is a collection of periodic orbits possessing the same qualitative features. For instance, the branch $S11+$ gathers all the periodic orbits for which the linear and nonlinear oscillators vibrate with the same frequency and in an in-phase fashion. There are two general classes of solutions: *symmetric solutions* $Snm\pm$ correspond to orbits that satisfy the initial conditions $\dot{v}(0) = \pm\dot{v}(T/2)$ and $\dot{y}(0) = \pm\dot{y}(T/2)$, where T is the period, n is the number of half-waves in v, and m the number of half-waves in y in a half-period interval; *unsymmetric solutions* Unm are orbits that fail to satisfy the initial conditions of the symmetric orbits, with the same notation for the two indices. We adopt the following convention regarding the placement of the various branches in the frequency domain: we assign to a specific branch

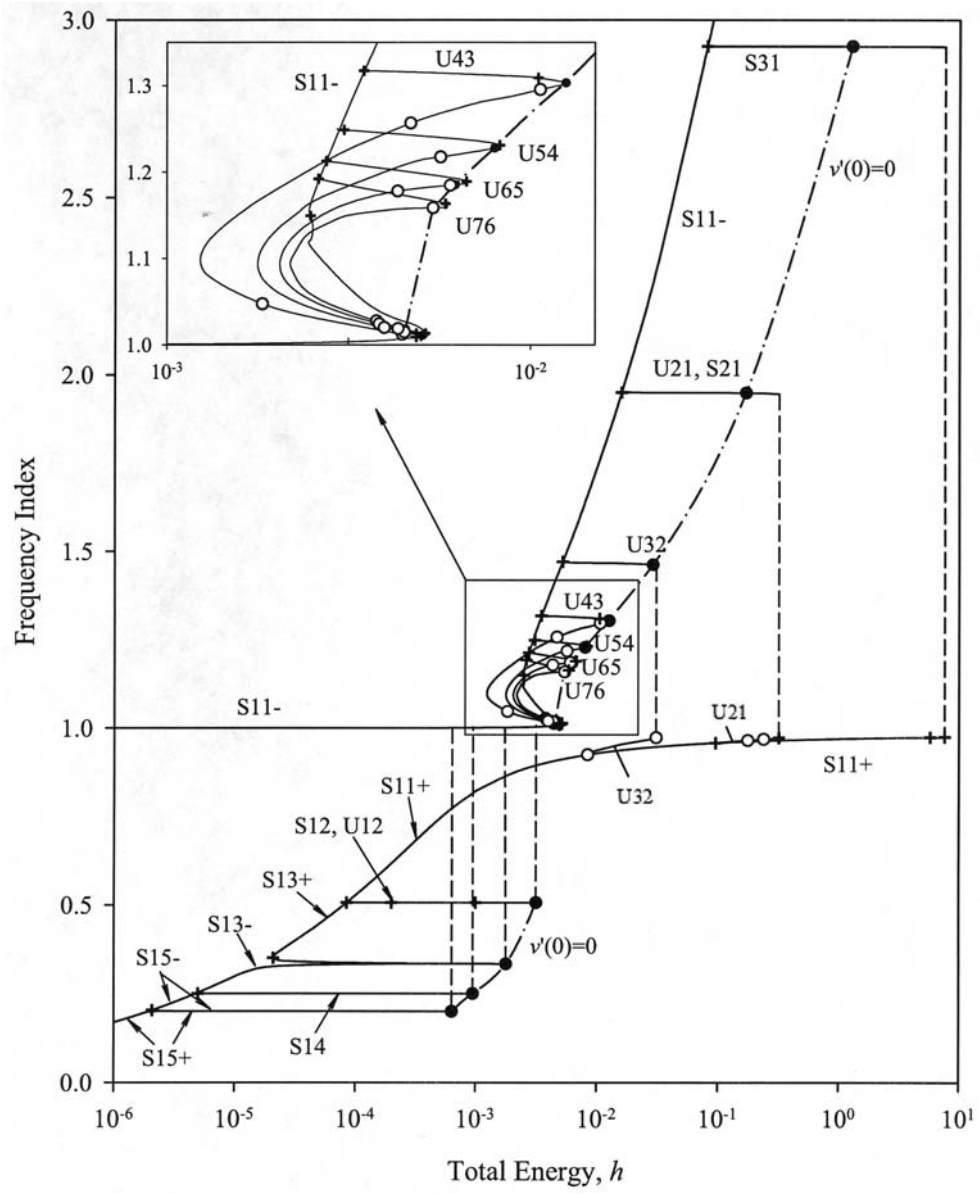

FIG. 1. *Frequency-energy plot of the periodic orbits: for the sake of clarity, no stability is indicated; special orbits are denoted by bullets* (•) *and are connected by dashed-dot lines; other symbols indicate bifurcation points (stability-instability boundaries):* (+) *four Floquet multipliers at* +1*, and* (◯) *two Floquet multipliers at* +1 *and two at* −1 *(see Lee et al.* (2005)*).*

of solutions a frequency index equal to the ratio of its indices; e.g., $S21\pm$ is represented by the frequency index $\omega = 2/1 = 2$, as is $U21$; $S13\pm$ is represented by $\omega = 1/3$; etc. This convention rule holds for every branch except $S11\pm$, which, however, are particular branches forming the basic backbone of the entire plot. On the energy axis we depict the (conserved) total energy of the system when it oscillates in the corresponding periodic motion. Transitions between certain branches seem to involve

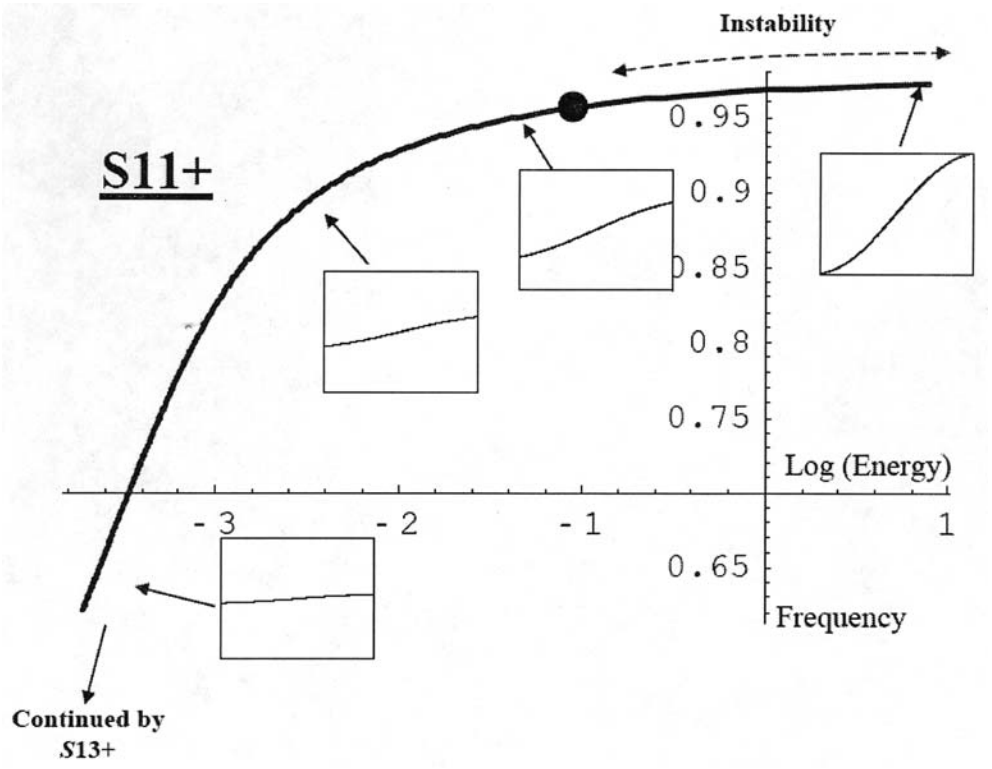

FIG. 2. *Detailed plot of branch* $S11+$ *in the frequency index-logarithm of energy plane. A dot* (•) *represents the initial condition of the motion depicted in Figure* 4. *(At certain points of the branch the corresponding motions in the configuration plane* (y, v) *are depicted.)*

"jumps," but this is only due to the frequency convention adopted, and no actual discontinuities in the dynamics occur. (By definition, branches $S(kn)(km)\pm$, k integer, are identified with $Snm\pm$.) Periodic orbits that correspond to synchronous motions of the two particles of the system, and correspond to curves in the configuration plane (y, v), will be termed *nonlinear normal modes (NNMs)* (Vakakis et al. (1996)).

The main backbone of the frequency-energy plot is formed by the branches $S11\pm$, which represent in- or out-of-phase NNMs possessing one half-wave per half-period. Moreover, the natural frequency of the linear oscillator $\omega_0 = 1$ (which we identify with a frequency index equal to unity, $\omega = 1$) naturally divides the periodic solutions into higher- and lower-frequency modes. A close-up of $S11+$ is presented in Figure 2 together with some modal curves depicted in the configuration plane (y, v) of the system. The horizontal and vertical axes in the plots in the configuration plane are the nonlinear and linear, respectively, oscillator responses, and the aspect ratios in these plots are set so that equal tick mark increments on the horizontal and vertical axes are equal in size, enabling one to directly deduce whether the motion is localized in the linear or the nonlinear oscillator. Figure 2 clearly highlights the energy dependence of the NNMs; the NNMs become strongly localized to the nonlinear attachment as the total energy in the system decreases. This observation shows how useful a frequency-energy plot can be for the interpretation of the dynamics. For the out-of-phase branch $S11-$, the NNMs become localized to y or v as $\omega \to 1+$ or $\omega \gg 1$, respectively.

There is a sequence of higher- and lower-frequency periodic solutions bifurcating

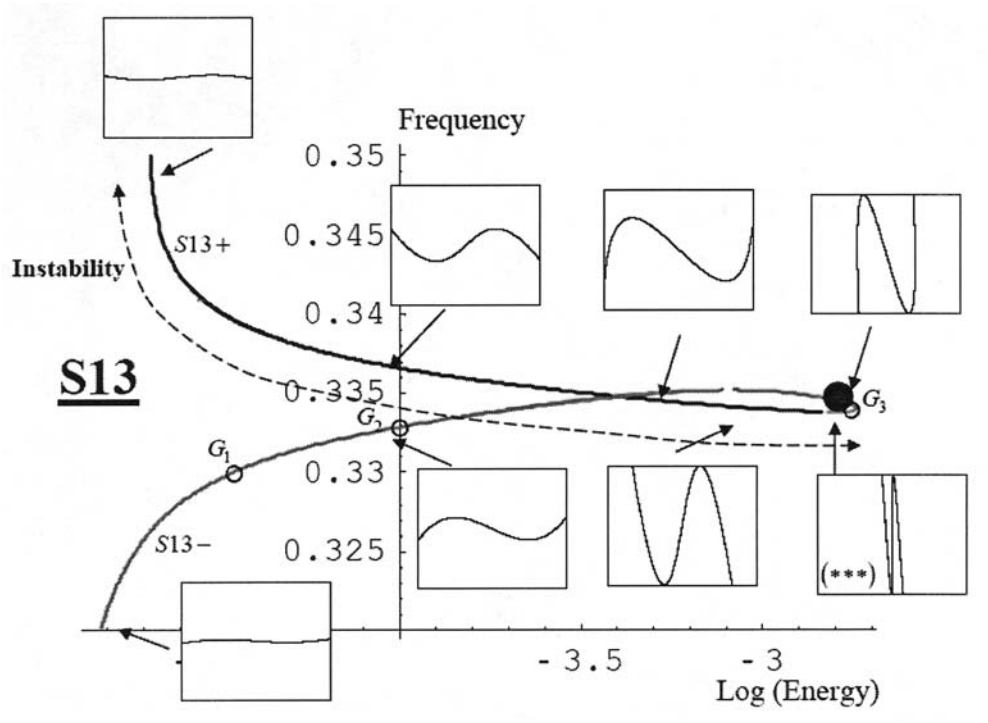

FIG. 3. *Detailed plot of tongues $S13\pm$ in the frequency index-logarithm of the energy plane. Points G_1, G_2, G_3 refer to the text, and the special periodic orbit is represented by triple stars $(***)$; the dot $(\bullet)$ represents the initial condition of the motion depicted in Figure 5. (At certain points of the branch the corresponding motions in the configuration plane (y, v) are depicted.)*

or emanating from branches $S11\pm$, which we will denote as *tongues*. Each tongue occurs in the neighborhood of an internal resonance between the linear oscillator and the nonlinear attachment, and corresponds to either symmetric (S-tongue; e.g., $S13\pm$) or unsymmetric (U-tongue; e.g., $U21\pm$) periodic motion of the system.

Considering first the symmetric solutions, the branches $S1(2k+1)\pm$, $k = 1, 2, \ldots$, appear in the neighborhoods of frequencies $\omega = 1/(2k+1)$, i.e., at progressively lower frequencies with increasing k. For fixed k, each of the two branches $S1(2k+1)\pm$ is linked through a smooth transition with its neighboring branches $S1(2k-1)\pm$ or $S1(2k+3)\pm$ and exists over a finite interval of energy. The pair $S1(2k+1)\pm$ is eliminated through a saddle-node bifurcation at a higher energy value (cf. Figure 3 for branches $S13\pm$). The pairs of branches $S1(2k)\pm$, $k = 1, 2, \ldots$, bifurcate out of $S1(2k+1)\pm$ and exist over finite energy intervals. Branches $Sn1\pm$, $n = 2, 3, \ldots$, appear in the neighborhoods of frequencies $\omega = n$, i.e., at progressively higher frequencies with increasing n; the pair of branches $Sn1\pm$ emanates from $S11-$ and coalesces with $S11+$ through a saddle-node bifurcation. Consider the subharmonic NNMs on tongues $S13\pm$ (similar results hold for the other S-branches), which correspond to motions where the linear oscillator oscillates "three times faster" than the nonlinear attachment. We refer to Figure 3, where a detailed frequency-energy plot for this branch is depicted.

We now discuss the evolution of the motion along $S13-$. As point G_1 is reached in the neighborhood of $\omega = 1/3$, it holds that $v(t) \gg y(t)$, and the nonlinear attachment

vibrates nearly independently, in essence "driving" the linear oscillator; moreover, at that regime of the motion the force generated by the essentially nonlinear coupling spring is approximately equal to that generated by the linear spring. As the energy increases towards point G_2 the nonlinear attachment still "drives" the primary mass, but now the force generated by the linear spring tends to overcome that of the nonlinear spring; this means that the motion of the linear oscillator is less influenced by the motion of the nonlinear attachment. Once point G_2 is reached (with initial displacements $v(0) = 0.0915$, $y(0) = 0.013$ and zero initial velocities), both the linear oscillator and the nonlinear attachment approximately vibrate as a set of *uncoupled linear oscillators* with natural frequencies at ratio 1/3,

$$\ddot{v} + \left(\frac{1}{9}\right) v = 0, \qquad \ddot{y} + y = 0.$$

This means that in the neighborhood of point G_2 of $S13-$ the system oscillates approximately as a system of two uncoupled linear oscillators, a result which explains why the branches $S13\pm$ appear as horizontal straight line segments at frequency index 1/3 of the frequency-energy plot of Figure 1. As energy increases towards point G_3 of Figure 2, the situation is reversed; because the force generated by the nonlinear spring is now negligible compared to that generated by the linear spring, the linear oscillator vibrates nearly independently and drives the nonlinear attachment. Eventually point G_3 is reached, where the periodic motion is approximately given by $y(t) \approx Y \cos \omega t$, $v(t) \approx V \cos \omega t$, and there occurs triple coalescence of branches $S13\pm$ and $S33-$ (which is identical to $S11-$).

Focusing now on the unsymmetric branches, we observe a family of $U(m+1)m$ branches bifurcating from branch $S11-$ that exist over finite energy levels and are eliminated through saddle-node bifurcations with other branches of solutions. The transition of branches $U21$ and $U32$ to $S11+$ seems to involve jumps, but this is only due to the frequency convention adopted, and no actual discontinuities in the dynamics occur. It should be mentioned that periodic motions on the U-tongues are not NNMs because nontrivial phases between the two oscillators are realized. The motion on these tongues is represented by Lissajous curves in the configuration plane, whereas motion on S-tongues corresponds to one-dimensional curves. Localization phenomena are also detected at certain regions of U-tongues (Lee et al. (2005)).

It turns out that certain periodic orbits (termed *special orbits* and depicted by dots in Figure 1) are of particular importance concerning the passive and irreversible energy transfer from the linear to the nonlinear oscillator. These special orbits satisfy the initial conditions $v(0) = \dot{v}(0) = y(0) = 0$ and $\dot{y}(0) \neq 0$, which happen to be identical to the state of the undamped system (1) at $t = 0+$ (being at rest at $t = 0-$) after application of an impulse of magnitude $\dot{y}(0)$ to the linear oscillator. Moreover, certain stable special orbits are localized to the nonlinear oscillator (Lee et al. (2005)) which implies that if the system initially at rest is forced impulsively and one of the stable, localized special orbits is excited, the major portion of the induced energy is channeled directly to the invariant manifold of that special orbit, and hence the motion is rapidly and passively transferred ("pumped") from the linear to the nonlinear oscillator. Therefore, *the impulsive excitation of one of the stable special orbits is one of the triggering mechanisms initiating (direct) passive energy pumping in the system.*

In the following section we discuss in detail three mechanisms for passive energy pumping in system (1). In addition to the mechanism based on excitation of special orbits, we analyze two energy pumping mechanisms that rely on the spatial localiza-

tion of the mode shapes of certain NNMs of Figure 1 as the energy of oscillation of the system decreases due to damping dissipation.

3. Energy pumping mechanisms in the damped system. In this section, the impulsively forced, damped system (1) is considered, and three basic mechanisms for the initiation of nonlinear energy pumping are studied. The first mechanism (*fundamental energy pumping*) is realized when the motion takes place along the backbone curve $S11+$ of the frequency-energy plot of Figure 1, occurring for relatively low frequencies $\omega < \omega_0$. The second mechanism (*subharmonic energy pumping*) resembles the first and occurs when the motion takes place along a lower frequency branch Snm, $n < m$. The third mechanism (*energy pumping initiated by nonlinear beat*), which leads to stronger energy pumping, involves the excitation of a special orbit with main frequency ω_{SO} greater than the natural frequency of the linear oscillator ω_0; in this case energy pumping is initiated by a nonlinear beat phenomenon, as discussed in the previous section. In what follows we discuss each mechanism separately, and provide numerical simulations that demonstrate passive and irreversible energy transfer from the linear oscillator to the nonlinear attachment in each case.

3.1. Fundamental energy pumping. The first mechanism for energy pumping involves excitation of the branch of in-phase synchronous periodic solutions $S11+$, where the linear oscillator and the nonlinear attachment oscillate with identical frequencies in the neighborhood of the fundamental frequency ω_0. Although energy pumping is considered only in the damped system, in order to gain an understanding of the governing dynamics it is necessary to consider the case of no damping.

In Figure 2 we depicted a detailed plot of branch $S11+$ of the undamped system and noted that, at higher energies, the in-phase NNMs are spatially extended (involving finite-amplitude oscillations of both the linear oscillator and the nonlinear attachment). However, *the nonlinear mode shapes of solutions on* $S11+$ *depend essentially on the level of energy, and at low energies they become localized to the attachment.* Considering now the motion in phase space, this low-energy localization is a basic characteristic of the two-dimensional NNM invariant manifold corresponding to $S11+$; moreover, this localization property is preserved in the weakly damped system, where the motion takes place in a two-dimensional damped NNM invariant manifold. This means that when the initial conditions of the damped system are such that they excite the damped analogue of $S11+$, the corresponding mode shape of the oscillation, initially spatially extended, becomes localized to the nonlinear attachment with decreasing energy due to damping dissipation. This, in turn, leads to passive, continuous, and irreversible transfer of energy from the linear oscillator to the nonlinear attachment which acts, in essence, as an NES. The underlying dynamical phenomenon governing fundamental energy pumping was proven to be a *resonance capture on a* 1:1 *resonance manifold* of the system (Vakakis and Gendelman (2001)).

Numerical evidence of fundamental energy pumping is given in Figure 4 for the system with parameters $\varepsilon = 0.05$, $\omega_0^2 = 1$, $C = 1$, and $\lambda_1 = \lambda_2 = 0.0015$. Small damping is considered in order to better highlight the energy pumping phenomenon, and the motion is initiated near the black dot of Figure 2. Comparing the transient responses of Figures 4(a)–(b), we note that the response of the primary system decays faster than that of the NES. The percentage of instantaneous energy captured by the NES versus time is depicted in Figure 4(e) and confirms the assertion that continuous and irreversible transfer of energy from the linear oscillator to the NES takes place; this is more evident by computing the percentage of total input energy that is eventually dissipated by the damper of the NES (cf. Figure 4(f)), which in this

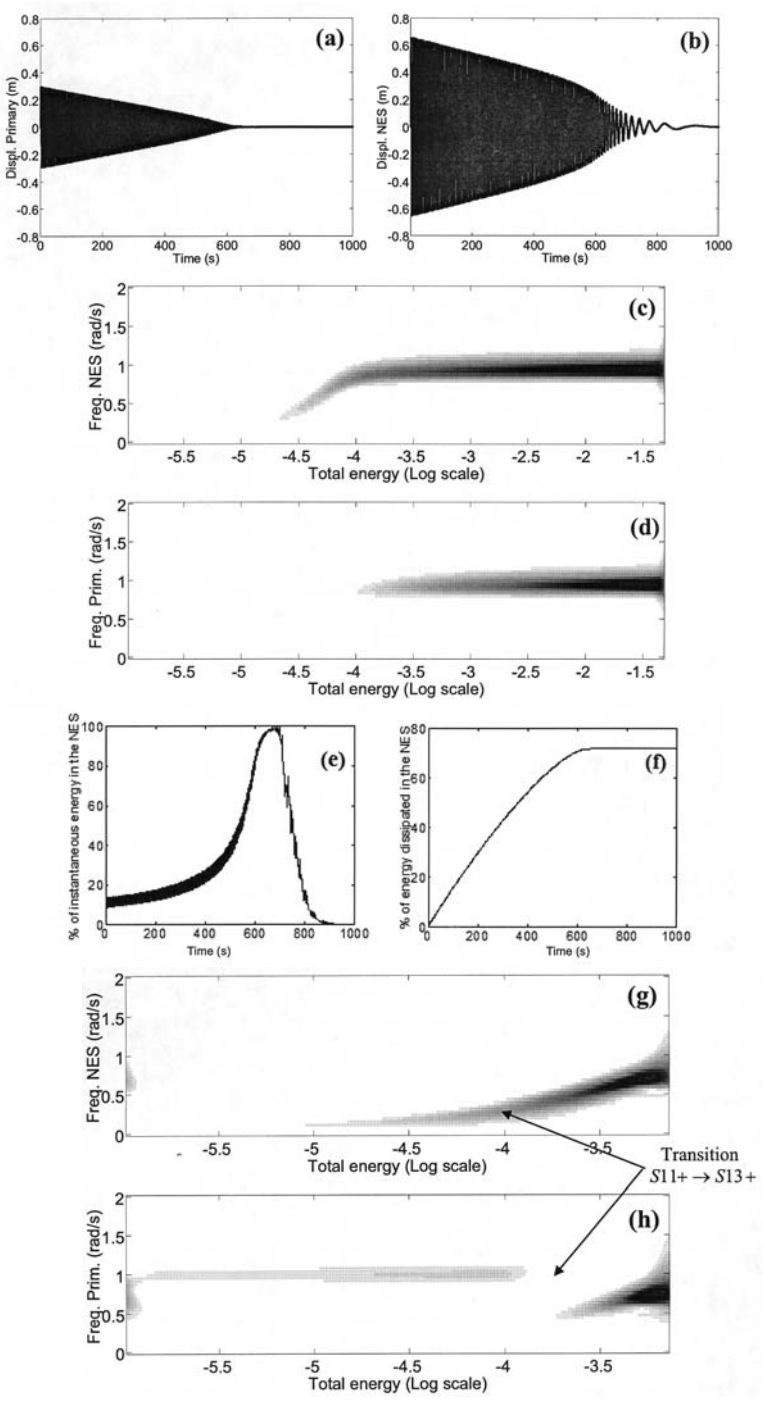

FIG. 4. *Fundamental energy pumping. Shown are the transient responses of the* (a) *linear oscillator and* (b) *NES; WTs of the motion of* (c) *NES and* (d) *linear oscillator;* (e) *percentage of instantaneous total energy in the NES;* (f) *percentage of total input energy dissipated by the NES; transition of the motion from* $S11+$ *to* $S13+$ *at smaller energy levels using the* (g) *NES (observe the settlement of the motion at frequency* 1/3*) and* (h) *linear oscillator.*

particular simulation amounts to 72%; the energy dissipated at the NES is computed by the relation

$$E_{NES}(t) = \lambda_2 \int_0^t \left[\dot{v}(\tau) - \dot{y}(\tau)\right]^2 d\tau.$$

The evolution of the frequency components of the motions of the two oscillators as energy decreases can be studied by numerical wavelet transforms (WTs) (Lee et al. (2005)) of the transient responses, as depicted in Figures 4(c)–(d). These plots highlight that a 1:1 resonance capture is indeed responsible for energy pumping. Below the value of -4 of the logarithm of energy level, the motion of the linear oscillator is too small to be analyzed by the particular windows used in the WT; however, a more detailed WT over smaller energy regimes (cf. Figures 4(g)–(h)) reveals a smooth transition from $S11+$ to $S13+$, in accordance with the frequency-energy plot of Figure 1. This transition manifests itself by the appearance of two predominant frequency components in the responses (at frequencies 1 and 1/3) as energy decreases.

3.2. Subharmonic energy pumping. Subharmonic energy pumping involves excitation of a low-frequency S-tongue. As mentioned previously, by low-frequency tongues we mean the particular regions of the frequency-energy plot where the NES engages in m:n (m, n integers such that $m < n$) resonance captures with the linear oscillator. Another feature of lower tongues is that in these regions the frequency of the motion remains approximately constant with varying energy; as a result, the tongues are represented by horizontal lines in the frequency-energy plot, and the response of system (1) resembles locally that of a linear system (see also discussion about the tongues $S13\pm$ in section 2). In addition, at each specific m:n resonance capture there appears a pair of closely spaced tongues corresponding to in- and out-of-phase oscillations of the two subsystems.

To discuss the dynamics of subharmonic energy pumping we now focus on a particular pair of lower tongues, say $S13\pm$, and refer to Figure 3. As discussed in section 2, at the extremity of a lower pair of tongues, the curve in the configuration plane is strongly localized to the linear oscillator. However, as for the fundamental mechanism for energy pumping, the decrease of energy by viscous dissipation leads to curves in the configuration plane that are increasingly localized to the NES, and nonlinear energy pumping to the NES occurs. In this case, the underlying dynamical phenomenon causing energy pumping is resonance capture in the neighborhood of an m:n resonance manifold of the dynamics. Specifically, for the pair of tongues $S13\pm$, a 1:3 resonance capture occurs that leads to subharmonic energy pumping with the linear oscillator vibrating with a frequency three times that of the NES. It is emphasized that due to the stability properties of the tongues $S13\pm$, subharmonic energy pumping involves excitation of $S13-$ but not of $S13+$.

The transient dynamics when the motion is initiated at the extremity of $S13-$ (cf. the initial condition denoted by the black dot in Figure 3) is displayed in Figure 5. The same parameters as in section 3.1 are considered. Until 500 s, subharmonic energy pumping takes place: despite the presence of viscous dissipation, the NES response grows continuously, with simultaneous rapid decrease of the response of the linear oscillator. A substantial amount of energy is transferred to the NES (cf. Figure 5(e)), and eventually nearly 70% of the energy is dissipated by the NES damper (cf. Figure 5(f)). A prolonged 1:3 resonance capture is nicely evidenced by the WT of Figures 5(c)–(d), and the motion follows the whole lower tongue $S13-$ from the right

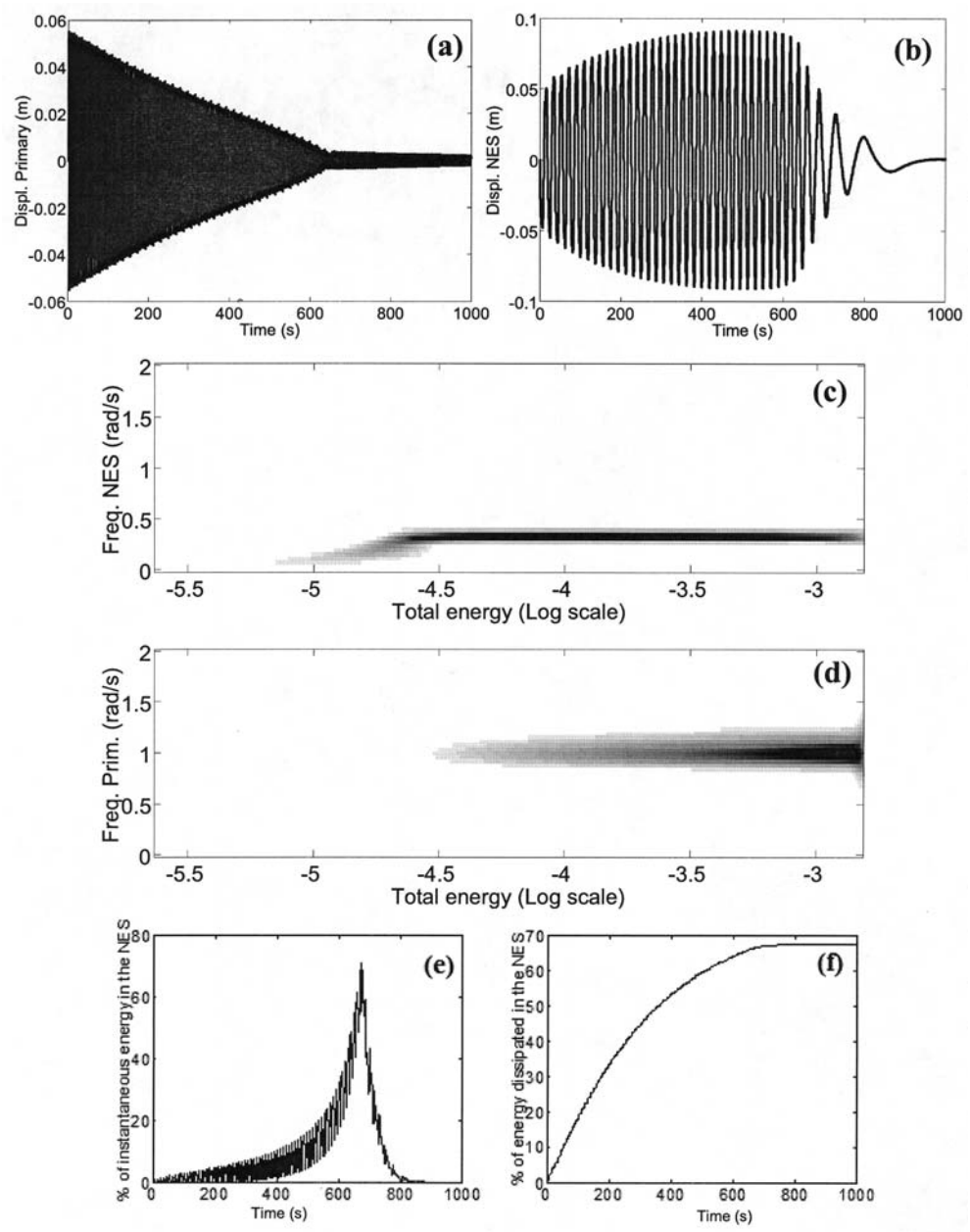

FIG. 5. *Subharmonic energy pumping initiated on S13−. Shown are the transient responses of the* (a) *linear oscillator and* (b) *NES; WTs of the motion of* (c) *the NES and* (d) *the linear oscillator;* (e) *percentage of instantaneous total energy in the NES;* (f) *percentage of total input energy dissipated by the NES.*

to the left. Once escape from resonance capture occurs (around 620–630 s), energy is no longer transferred to the NES.

3.3. Energy pumping initiated by nonlinear beating. The previous two mechanisms cannot be activated with the NES at rest, since in both cases the motion

is initialized from a nonlocalized state of the system. This means that these energy pumping mechanisms cannot be activated directly after the application of an impulsive excitation to the linear oscillator with the NES initially at rest. Such a forcing situation, however, is important from a practical point of view; indeed, this is the situation where local NESs are utilized to confine and passively dissipate unwanted vibrations from linear structures that are forced by impulsive (or broadband) loads.

Hence, it is necessary to discuss an alternative, third energy pumping mechanism capable of initiating passive energy transfer with the NES being initially at rest. This alternative mechanism is based on the excitation of a *special orbit* (as defined and discussed in section 2) that plays the role of a "bridging orbit" for activation of either fundamental or subharmonic energy pumping. Excitation of a special orbit results in the transfer of a substantial amount of energy from the initially excited linear oscillator directly to the NES through a nonlinear beat phenomenon. In that context, the special orbit may be regarded as an initial bridging orbit or trigger, which eventually activates fundamental or subharmonic energy pumping, once the initial nonlinear beat initiates the energy transfer. Indeed, as shown below, *the third mechanism for energy pumping represents an efficient initial (triggering) mechanism for rapid transfer of energy from the linear oscillator to the NES at the crucial initial stage of the motion, before activating either one of the (fundamental or subharmonic) main energy pumping mechanisms through a nonlinear transition (jump) in the dynamics.*

To study the dynamics of this triggering mechanism, we first formulate the following conjecture: *Due to the essential (nonlinearizable) nonlinearity, the NES is capable of engaging in an m:n resonance capture with the linear oscillator, m and n being a set of integers. Accordingly, in the undamped system there exists a sequence of special orbits (corresponding to nonzero initial velocity of the linear oscillator with all other initial conditions zero), aligned along a one-dimensional smooth manifold in the frequency-energy plot.* As a first step to test this conjecture, a nonlinear boundary value problem (NLBVP) was formulated to compute the periodic orbits of system (1) with no forcing and damping, and the additional restriction for the special orbits was imposed. (For a detailed formulation of the NLBVP, we refer to Lee et al. (2005).) The numerical results in the frequency-energy plane are depicted in Figure 6 for parameters $\varepsilon = 0.05$, $\omega_0^2 = 1$, $C = 1$. Each triangle in the plot represents a special orbit, and a one-dimensional manifold appears to connect the special orbits (though a rigorous proof of the existence of this manifold is not given here). In addition, it appears that there exists a countable infinity of special orbits, occurring in the neighborhoods of the countable infinities of internal resonances m:n (m, n integers) of the system, but again no rigorous proof of this conjecture is given in this paper. We note that a subset of high-frequency branches (for $\omega > 1$) possesses two special orbits instead of one (for example, all $U(p+1)p$ branches with $p \geq 3$). To distinguish between the two special solutions in such high-frequency branches we partition them into two subclasses: the a-special orbits, which exist in the neighborhood of $\omega = \omega_0 = 1$, and the b-special orbits, which occur away from this neighborhood (cf. Figure 6); it was numerically proven in Lee et al. (2005) that the a-special orbits are unstable, whereas the b-special orbits are stable. As shown below, it is the excitation of the stable b-special orbits that activates the third mechanism for energy pumping.

Representative special orbits are given in Figure 7. By construction, all special orbits have a common feature; namely, they pass with vertical slope through the origin of the configuration plane (y, v). This feature renders them compatible with an impulse applied to the linear oscillator, which corresponds to a nonzero velocity of the linear oscillator with all other initial conditions zero. The curves corresponding to

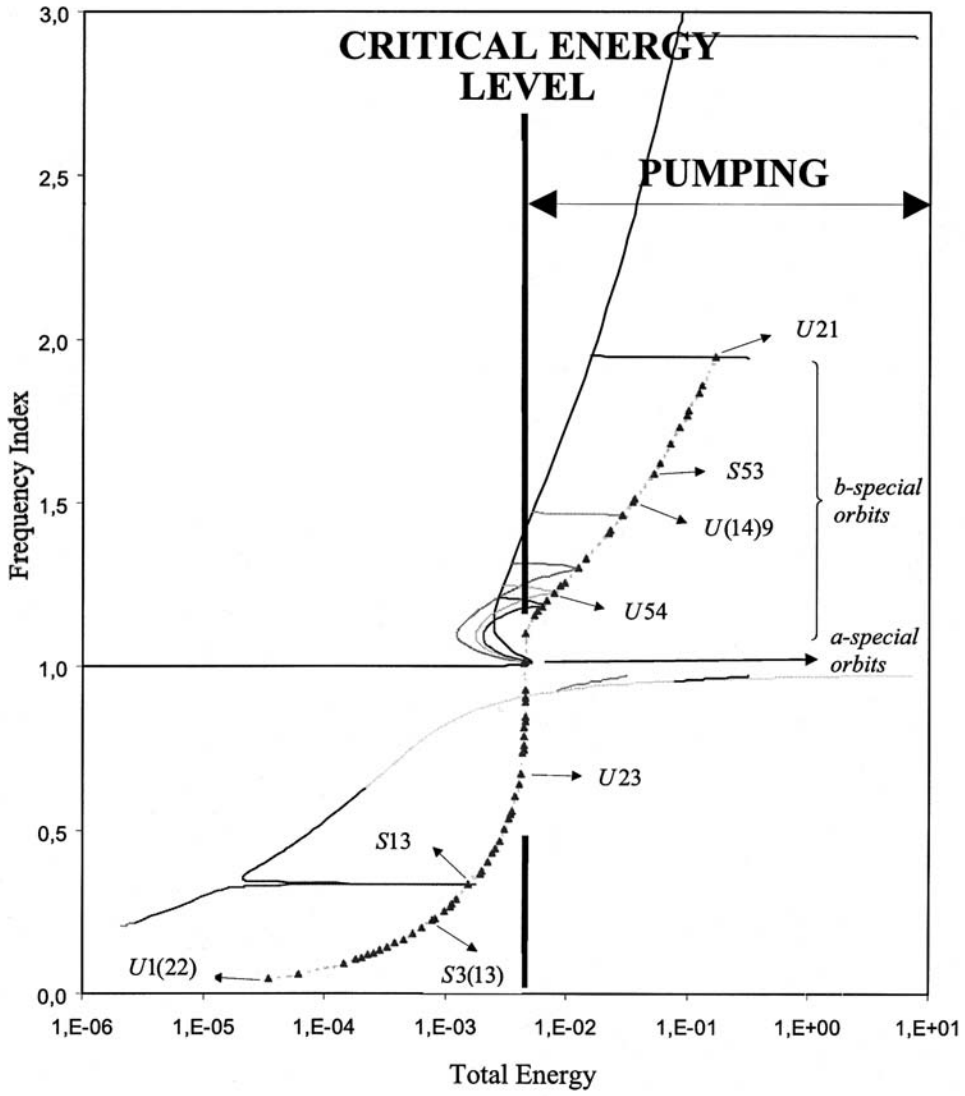

FIG. 6. *Manifold of special orbits (represented by triangles) in the frequency-energy plot.*

the special orbits in the configuration plane can be either closed or open, depending upon the differences between the two indices characterizing the orbits; specifically, odd differences between indices correspond to closed curves in the configuration plane and lie on U-branches, whereas even differences between indices correspond to open curves on S-branches. In addition, higher-frequency special orbits (with frequency index $\omega > \omega_0$) in the upper part of the frequency-energy plot (i.e., $m > n$) are localized to the nonlinear oscillator; conversely, special orbits in the lower part of the frequency-energy plot (with frequency index $\omega < \omega_0$) tend to be localized to the linear oscillator. This last observation is of particular importance since it directly affects the transfer of a significant amount of energy from the linear oscillator to the NES through the mechanism discussed in this section: indeed, there seems to be a well-

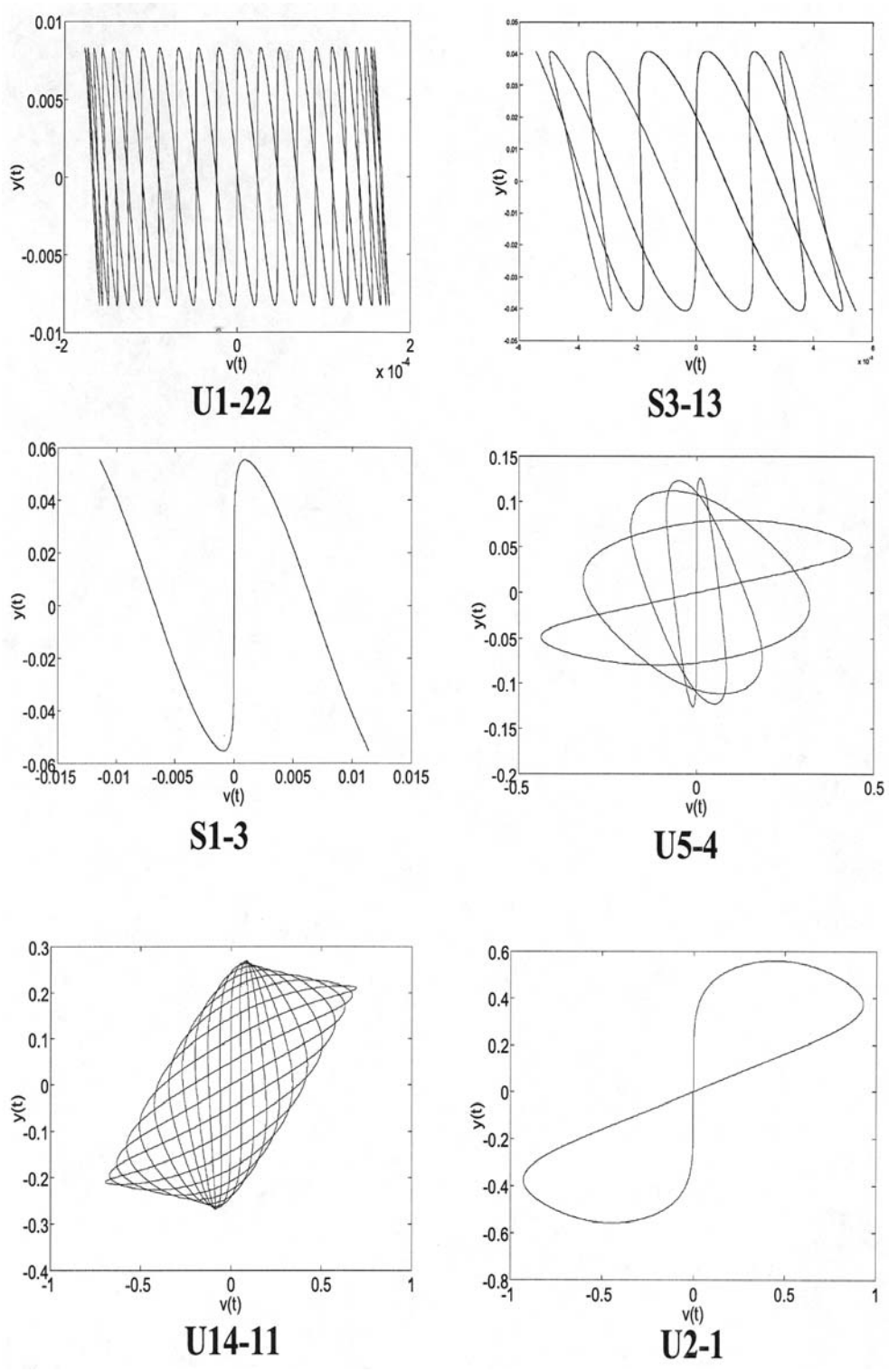

FIG. 7. *Representative special orbits in the configuration plane* (y, v). *Closed curves correspond to special orbits on* U*-branches, and open curves to special orbits on* S*-branches.*

defined critical threshold of energy that separates high- from low-frequency special orbits, i.e., those that do or do not localize, respectively, to the NES (cf. Figure 6). *The third mechanism for energy pumping can be activated only for input energies above the critical threshold*, since below that the (low-frequency) special orbits are incapable of transferring significant amounts of input energy from the linear oscillator to the NES; in other words, the critical level of energy represents a lower bound below which no significant energy pumping can be initiated through activation of a special orbit. Moreover, combining this result with the topology of the one-dimensional manifold of special orbits of Figure 6, it follows that *it is the subclass of stable b-special orbits that is responsible for activating the third energy pumping mechanism, whereas the subclass of unstable a-special orbits does not affect energy pumping.* This theoretical insight will be fully validated by the numerical simulations that follow.

We now proceed to analyze in detail the nonlinear beat phenomenon that takes place when a special orbit is excited by the initial conditions. When the NES engages in an m:n resonance capture with the linear oscillator, a nonlinear beat phenomenon takes place. Due to the essential (nonlinearizable) nonlinearity of the NES and the lack of any preferential frequency, the considered nonlinear beat phenomenon does not require any a priori "tuning" of the nonlinear attachment, since at the specific frequency-energy range of the m:n resonance capture the nonlinear attachment adjusts its amplitude ("tunes itself") to fulfill the necessary conditions of internal resonance. This represents a significant departure from the classical nonlinear beat phenomenon observed in coupled oscillators with linearizable nonlinear stiffnesses (e.g., spring-pendulum systems), where the defined ratios of linearized natural frequencies of the component subsystems dictate the type of internal resonances that can be realized (Golnaraghi (1991), Salemi, Golnaraghi, and Heppler (1997)). As an example, in Figure 8 we depict the exchanges of energy during the nonlinear beat phenomena corresponding to the special orbits of branches $U21$ and $U54$ for parameters $\varepsilon = 0.05$, $\omega_0^2 = 1$, $C = 1$ and no damping. As expected, energy is continuously exchanged between the linear oscillator and the NES, so the energy transfer is not irreversible as is required for energy pumping; *we conclude that excitation of a special orbit can only initiate (trigger) energy pumping, but not cause it in itself.* The amount of energy transferred during each cycle of the beat varies with the special orbit considered; for $U21$ and $U54$, as much as 32% and 86% of energy, respectively, can be transferred to the NES. It can be shown that, for increasing integers m and n with corresponding ratios $m/n \to 1+$, the maximum energy transferred during a cycle of the special orbit tends to 100%; at the same time, however, the resulting period of the cycle of the beat (and, hence, of the time needed to transfer the maximum amount of energy) should increase as the least common multiple of m and n.

We note at this point that the nonlinear beat phenomenon associated with the excitation of the special orbits can be studied analytically using the complexification-averaging method first introduced by Manevitch (1999). To demonstrate the analytical procedure, we analyze in detail the special orbit on branch $U21$ of the system with no damping. In Lee et al. (2005), the periodic motions on this entire branch were studied, and it was shown that the responses of the linear oscillator and the nonlinear attachment can be approximately expressed as

$$\begin{aligned} y(t) &= Y_1 \sin \omega t + Y_2 \sin 2\omega t \equiv y_1(t) + y_2(t), \\ v(t) &= V_1 \sin \omega t + V_2 \sin 2\omega t \equiv v_1(t) + v_2(t), \end{aligned} \tag{2}$$

where

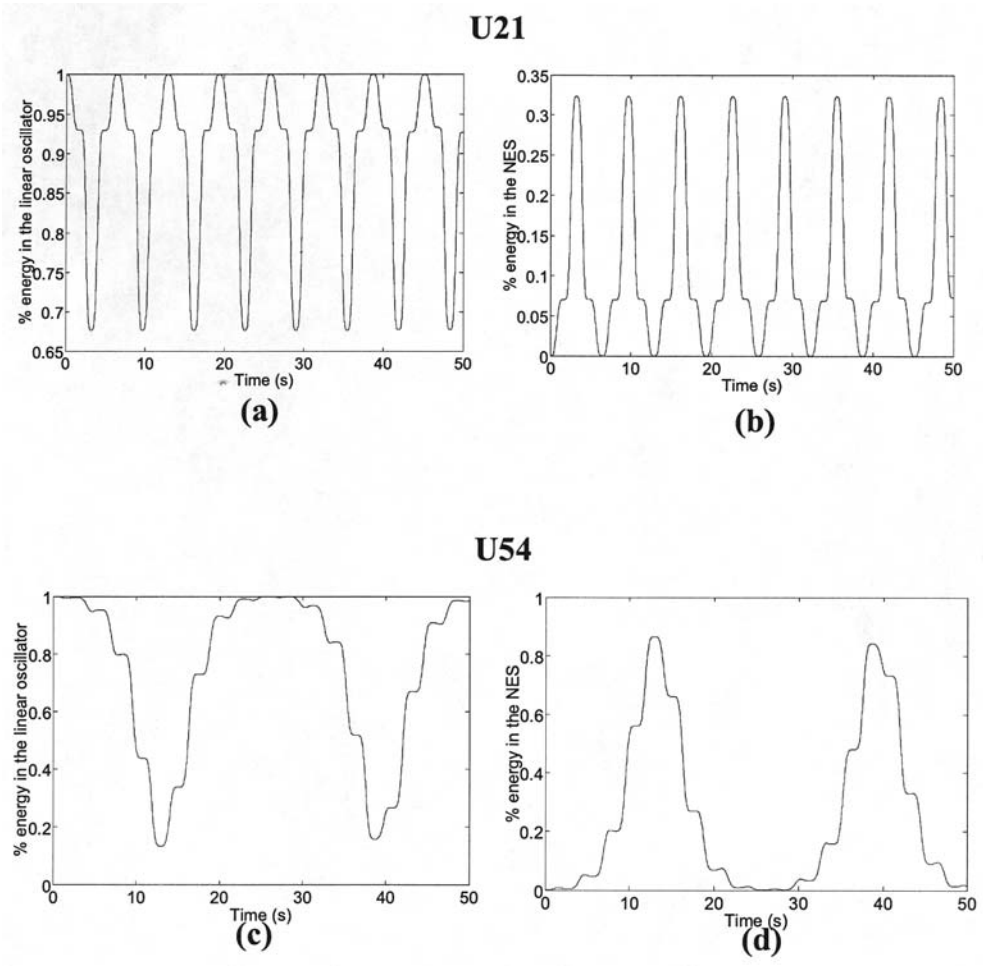

FIG. 8. *Exchanges of energy during nonlinear beat phenomena corresponding to special orbits on* (a), (b) $U21$, *and* (c), (d) $U54$.

$$A = \frac{\varepsilon\omega^2}{\omega_0^2 - \omega^2} B \quad \text{and} \quad D = \frac{4\varepsilon\omega^2}{\omega_0^2 - 4\omega^2} G,$$

$$B = \pm\sqrt{\frac{4\varepsilon\omega^4(Z_2 - 8Z_1)}{9CZ_1^3 Z_2}} \quad \text{and} \quad G = \pm\sqrt{\frac{32\varepsilon\omega^4(2Z_1 - Z_2)}{9CZ_2^3 Z_1}},$$

$$Z_1 = \frac{\varepsilon\omega^2}{\omega_0^2 - \omega^2} - 1 \quad \text{and} \quad Z_2 = \frac{4\varepsilon\omega^2}{\omega_0^2 - 4\omega^2} - 1,$$

$$Y_1 = \frac{A}{\omega}, \quad V_1 = \frac{B}{\omega}, \quad Y_2 = \frac{D}{2\omega}, \quad V_2 = \frac{G}{2\omega}.$$

Hence, a two-frequency approximation is satisfactory for this family of periodic motions. The frequency ω_{SO} at which the special orbit appears is computed by imposing the initial conditions $y(0) = v(0) = \dot{v}(0) = 0$, which leads to the relation

$$B = -2G \qquad \text{(special orbit)}.$$

The instantaneous fraction of total energy in the linear oscillator during the nonlinear beat phenomenon is estimated to be

$$E_{linear}(t) = \frac{\left[(\omega_0^2 - 4\omega_{SO}^2)\sin\omega_{SO}t - 2(\omega_0^2 - \omega_{SO}^2)\sin 2\omega_{SO}t\right]^2}{9\omega_{SO}^2\omega_0^2} + \frac{\left[(\omega_0^2 - 4\omega_{SO}^2)\cos\omega_{SO}t - 4(\omega_0^2 - \omega_{SO}^2)\cos 2\omega_{SO}t\right]^2}{9\omega_0^4}. \tag{3}$$

The nonlinear coefficient C has no influence on the fraction of total energy transferred to the NES during the nonlinear beat; this means that, during the beat, the instantaneous energies of the linear oscillator and the NES are directly proportional to the nonlinear coefficient. Moreover, as the mass of the NES tends to zero, the frequency where the special orbit is realized tends to the limit $\omega_{SO} \to \omega_0$, and, as a result, $E_{linear}(t) \to 1$, and the energy transferred to the NES during the beat tends to zero. However, we note that this is a result satisfied only asymptotically, since, as indicated by the results depicted in Figure 8, even for very small mass ratios, i.e., $\varepsilon = 0.05$, as much as 86% of the total energy can be transferred to the NES during a cycle of the special orbit of branch $U54$.

Considering now the damped system, we will show that following an initial nonlinear beat phenomenon, either one of the main (fundamental or subharmonic) energy pumping mechanisms can be activated through a nonlinear transition (jump) in the dynamics. It was previously mentioned that the two main energy pumping mechanisms are qualitatively different from the third mechanism, which is based on the excitation of a nonlinear beat phenomenon (special orbit); indeed, damping is a prerequisite for the realization of the two main mechanisms, leading to an irreversible energy transfer from the linear oscillator to the NES, whereas a special orbit is capable of transferring energy without dissipation, though this transfer is not irreversible but periodic. This justifies our earlier assertion that the third mechanism does not represent an independent mechanism for energy pumping, but rather triggers it, and through a nonlinear transition activates either of the two main mechanisms. This will become apparent in the following numerical simulations.

The following simulations concern the transient dynamics of the damped system (1) with parameters $\varepsilon = 0.05$, $\omega_0^2 = 1$, $C = 1$, $\lambda_1 = \lambda_2 = 0.0015$ and an impulse of magnitude Y applied to the linear oscillator (corresponding to initial conditions $y(0+) = v(0+) = \dot{v}(0+) = 0$, $\dot{y}(0+) = Y$). By varying the magnitude of the impulse we study the different nonlinear transitions that take place in the dynamics and their effects on energy pumping. The responses of the system to the relatively strong impulse $Y = 0.25$ are depicted in Figure 9. Inspection of the WTs of the responses (cf. Figures 9(c)–(d)), and of the portion of total instantaneous energy captured by the NES (cf. Figure 9(e)), reveals that at the initial stage of the motion (until approximately $t = 120$ s) the (stable) b-special orbit on branch $U32$ is excited (since the NES response possesses two main frequency components at 1 and 3/2 rad/s), and a nonlinear beat phenomenon takes place. (Note the continuous exchange of energy between the two subsystems—reversibility in this initial stage of the motion.) For $t > 120$ s, the dynamics undergoes a transition (jump) to branch $S11+$, and fundamental energy pumping to the NES occurs on a prolonged 1:1 resonance capture (cf. Figures 9(c)–(d)); eventually, 84% of the input energy is dissipated by the damper of the NES (cf. Figure 9(f)).

Lowering the magnitude of the impulse to $Y = 0.11$ gives rise to a different set of nonlinear transitions, as the simulations of Figure 10 indicate. In this case the (stable)

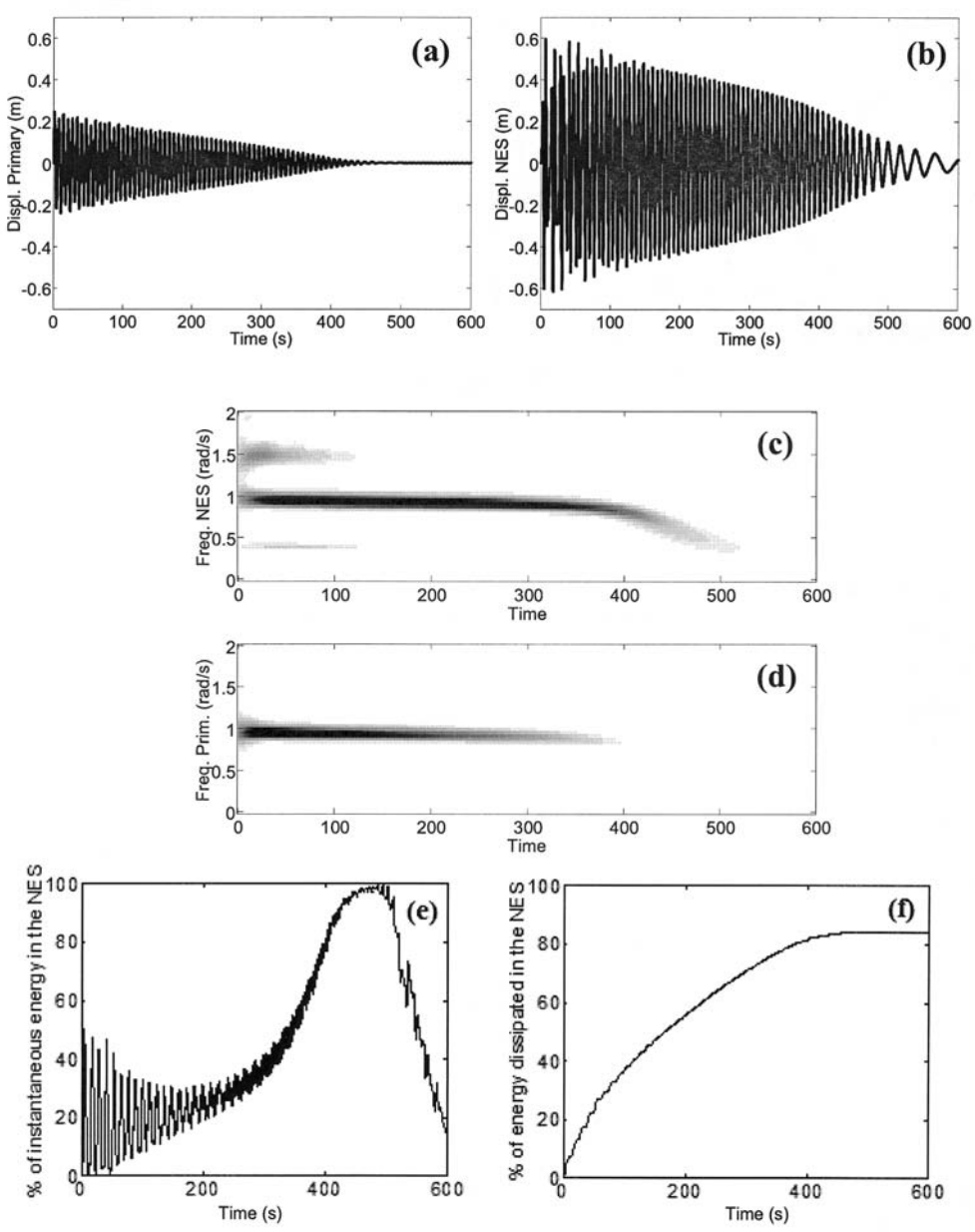

FIG. 9. *Energy pumping by nonlinear beat, transition to* $S11+$. *Shown are transient responses of* (a) *the linear oscillator and* (b) *NES; WTs of the motion of* (c) *NES and* (d) *the linear oscillator;* (e) *percentage of instantaneous total energy in the NES;* (f) *percentage of total input energy dissipated by the NES.*

b-special orbit of branch $U43$ is initially excited, which then activates subharmonic energy pumping through a nonlinear transition to the tongue $S13-$. In other words, the lower tongue appears to act as "bait" and activates energy pumping through 1:3 resonance capture, i.e., by capturing locally the transient dynamics in its domain of attraction. Figure 10(e) reveals that a nonlinear beat phenomenon occurs until

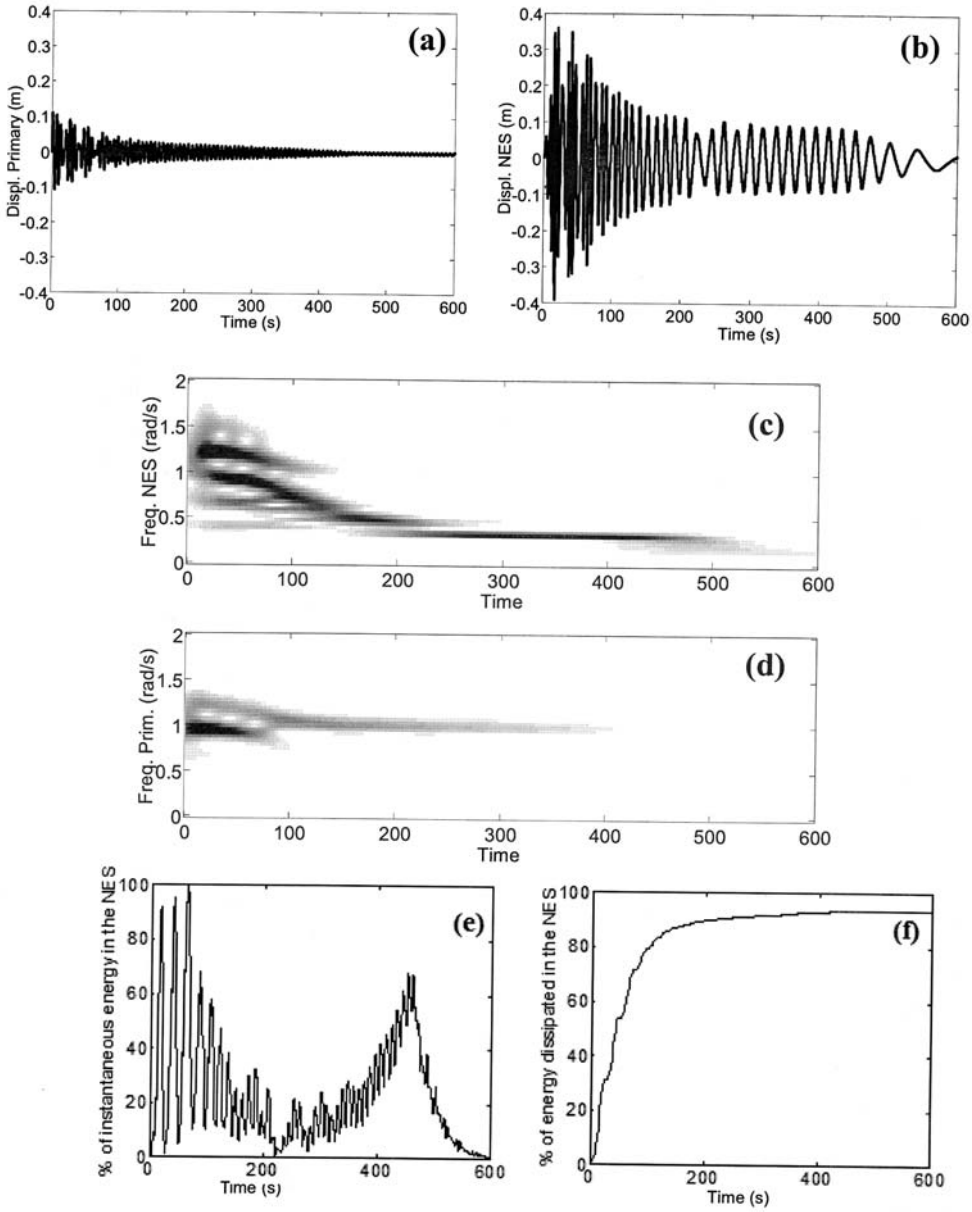

FIG. 10. *Energy pumping by nonlinear beat, transition to* $S13-$. *Shown are transient responses of* (a) *the linear oscillator and* (b) *NES; WTs of the motion of* (c) *NES and* (d) *the linear oscillator;* (e) *percentage of instantaneous total energy in the NES;* (f) *percentage of total input energy dissipated by the NES.*

$t = 150$ s approximately, and in turn activates 1:3 subharmonic energy pumping to the NES (cf. Figures 10(c)–(d)); eventually, 94% of the input energy is dissipated by the NES (cf. Figure 10(f)).

Comparing the two simulations, we conclude that excitation of the *b*-special orbit of $U43$ leads to more effective energy pumping compared to the *b*-special orbit of $U32$. The reason rests with the localization properties of the special orbits, i.e.,

their capacity to transfer a larger fraction of the total energy to the NES during a cycle of the oscillation. Indeed, the localization properties of the b-special orbits of branches $U(p+1)p$ are enhanced as the order p increases, i.e., as their second frequency component, $\omega = (p+1)/p$, approaches that of the first, $\omega = 1$, and the special orbits topologically approach the branch $S11-$ (Lee et al. (2005)). In that context, the b-special orbit of $U43$ is capable of transferring a larger fraction of the input than that being transferred by the b-special orbit of $U32$ (compare Figures 9(e) and 10(e)), and hence the enhanced energy pumping results of the second simulation. We note at this point that the (unstable) a-special orbits of these branches are localized in the linear oscillator and do not affect energy pumping.

We now test the previous theoretical finding that, for sufficiently small impulse magnitudes, no energy pumping can occur, i.e., none of the three aforementioned energy pumping mechanisms can be activated. The simulations for $Y = 0.08$ are depicted in Figure 11. The WT of the NES response of Figure 11(c) shows the presence of a frequency component below $\omega = 1$ at the initial stage of the motion, which indicates excitation of a low-frequency special orbit in the lower part ($\omega < 1$) of the frequency-energy plot (i.e., $U12$). As explained previously, those orbits are localized to the linear oscillator and, as a result, cannot transfer a sufficient amount of energy to the NES in the initial stage of the motion. Accordingly, neither the fundamental nor the subharmonic energy pumping mechanism is eventually activated, leading to a much smaller amount of energy dissipated by the NES (around 45% in this case). This result confirms our previous assertion that energy pumping through nonlinear beat can be activated only above a critical energy threshold (cf. Figure 6).

To demonstrate more clearly the effect of the b-special orbits on energy pumping, in Figure 12 we depict the percentage of input energy eventually dissipated at the NES for varying magnitudes of the impulse for the system with parameters $\varepsilon = 0.05$, $\omega_0^2 = 1$, $C = 1$, $\lambda_1 = \lambda_2 = 0.01$. In the same plot we depict the positions of the special orbits of the undamped system and the critical threshold predicted in Figure 6. We conclude that strong energy pumping is associated with the excitation of b-special orbits of the branches $U(p+1)p$ in the neighborhood above the critical threshold, whereas excitation of a-special orbits below the critical threshold does not lead to rigorous energy pumping. As mentioned previously, in the neighborhood of the critical threshold the b-special orbits are strongly localized to the NES, whereas a-orbits are nonlocalized. We also note from Figure 12 the deterioration of energy pumping as we increase the magnitude of the impulse well above the critical threshold, where high-frequency special orbits are excited; this is a consequence of the fact that well above the critical threshold the special orbits are weakly localized to the NES.

Extending the previous result, in Figure 13 we depict the contours of energy eventually dissipated at the NES, but now for the case of two impulses of magnitudes $\dot{y}(0)$ and $\varepsilon\dot{v}(0)$ applied to both the linear oscillator and the NES, respectively. The system parameters used were identical to those of the previous simulation of Figure 12. Superimposed on contours of energy dissipated at the NES are certain high- and low-frequency U- and S-branches of the undamped system together with their special orbits, in order to confirm for this case the essential role of the high-frequency special orbits in energy pumping. Indeed, high levels of energy dissipation are encountered in neighborhoods of contours of high-frequency U-branches, whereas low values are noted in the vicinity of low-frequency branches. These results agree qualitatively with our earlier theoretical and numerical findings and enable us to assess and establish the robustness of energy pumping when the NES is not initially at rest.

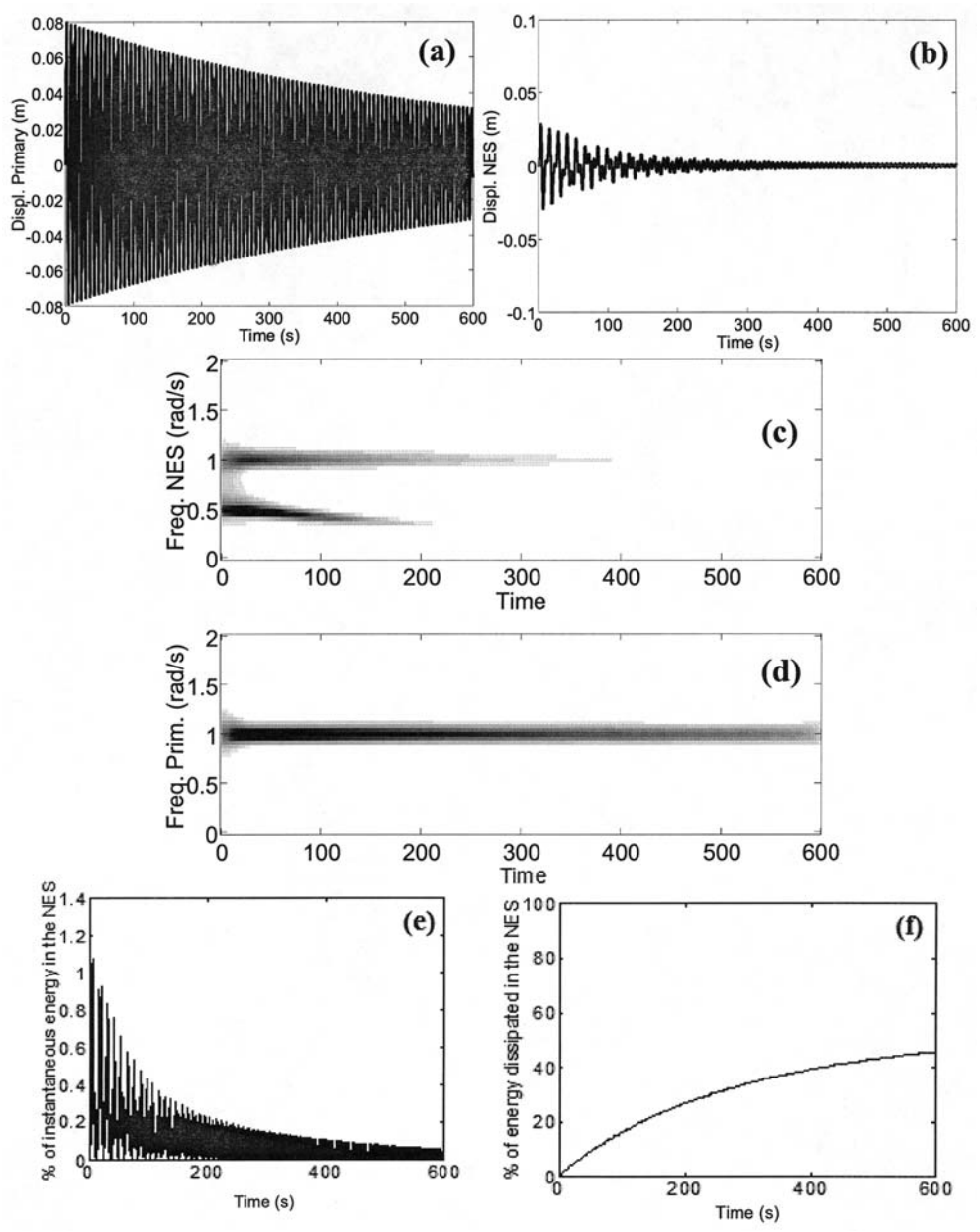

FIG. 11. *Absence of energy pumping for low excitation. Shown are transient responses of* (a) *the linear oscillator and* (b) *NES; WTs of the motion of* (c) *NES and* (d) *the linear oscillator;* (e) *percentage of instantaneous total energy in the NES;* (f) *percentage of total input energy dissipated by the NES.*

In the next section we provide analytical studies of the fundamental and subharmonic energy pumping mechanisms encountered in the damped system; since excitation of nonlinear beats is merely a means for activating the main two energy pumping mechanisms, it will not be analyzed below. We show that in each case we can reduce the governing dynamics of energy pumping to low-order slow-flow dynamical systems.

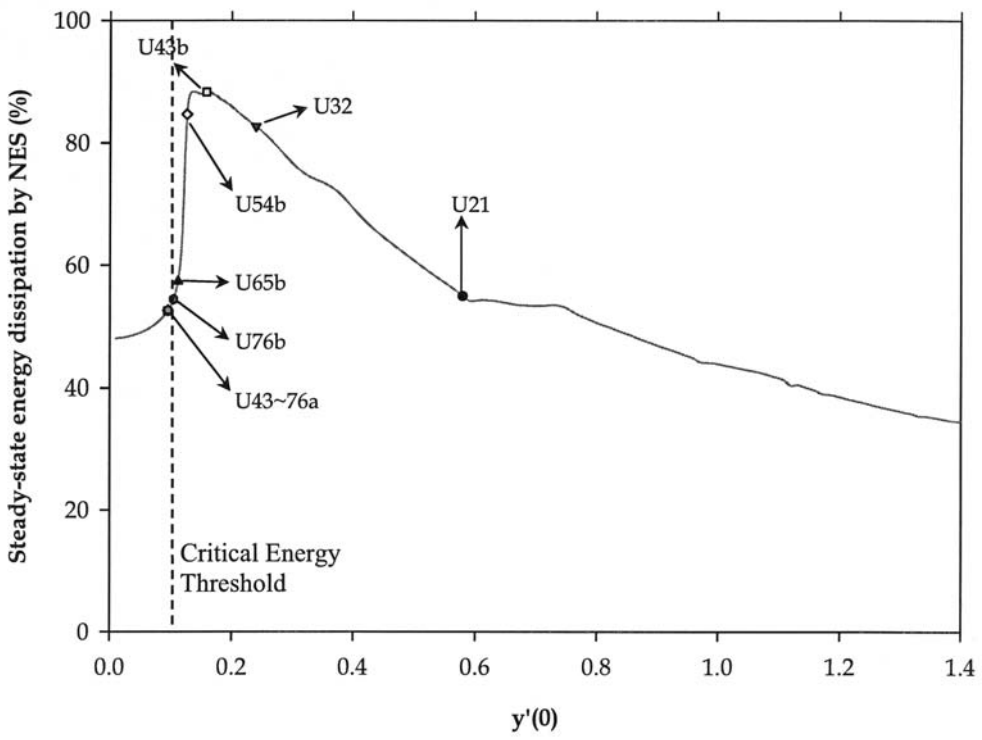

FIG. 12. *Percentage of input energy eventually dissipated at the NES for varying magnitudes of the impulse (the positions of certain special orbits are indicated).*

4. Slow-flow analysis. We now focus on the resonance capture dynamics that governs energy pumping in the damped system. This can be studied by performing a reduction of the dynamics, an approximate partition between slow and fast dynamics, and considering the evolution of the slow-flow dynamics when energy pumping takes place. We show that even though the system of coupled oscillators possesses essential (nonlinearizable) stiffness nonlinearities, analytical modeling of its dynamics at certain motion regimes can still be performed.

The theory of resonance processes for multifrequency systems was developed by Neishtadt (1997), (1999), where capture into and scattering on the resonance were discussed by considering them as random events and computing probabilities of capture and probabilistic distributions of the scattering amplitudes. By assuming small perturbations (e.g., weak nonlinearities), action-angle formulations and the averaging theorem were applied to provide analytical asymptotic validity of the approximations. Also, by introducing a mapping (called the *in-out function*) from a state of resonance capture to that of escape, glued averaging approximation was utilized to analytically describe motions when they are away from, captured into, and escaped from the resonance manifold.

Similar formulations were considered in Vakakis and Gendelman (2001), where the slow-flow equations were established also by the complexification/averaging technique. This method does not necessarily require the perturbations to be small, although it is similar to the (classical) averaging method; once the proper ansatz regarding the frequency content of the response is included, it is numerically verified that the

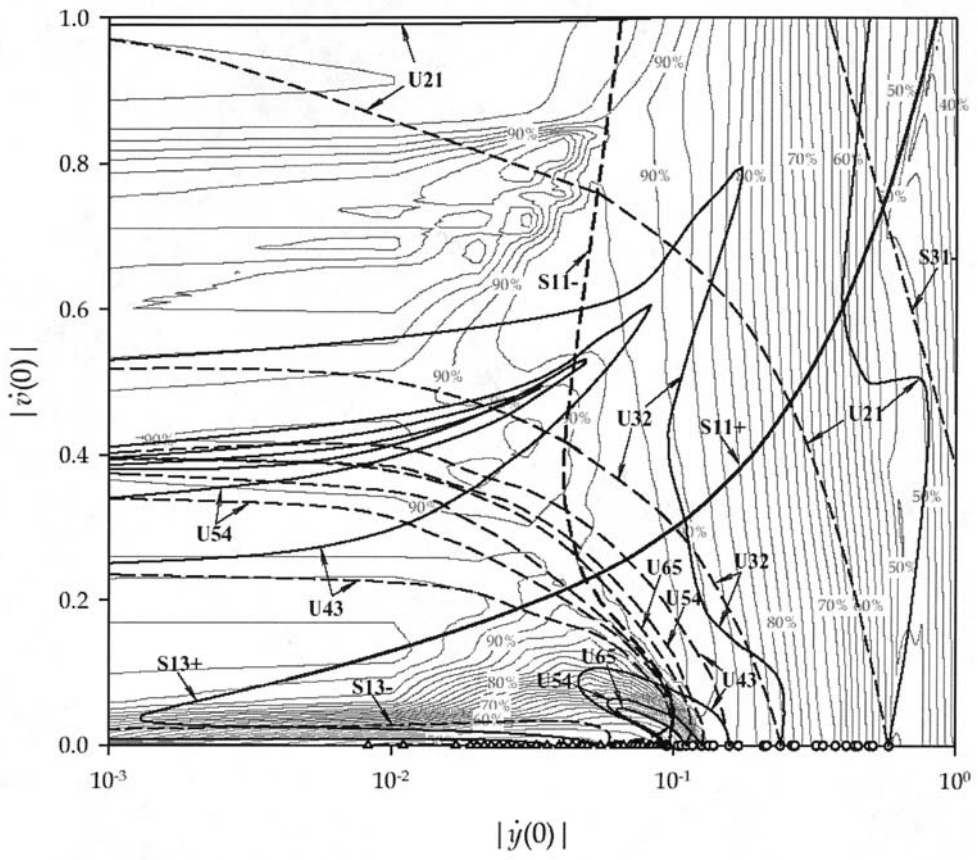

FIG. 13. *Contours of percentages of input energy eventually dissipated at the NES for the case when both oscillators are excited by impulses: superimposed are contours of high- and low-frequency branches of the undamped system (solid line: in phase, dashed line: out of phase branches); special curves in high- and low-frequency branches are denoted by* (◯) *and* (Δ)*, respectively.*

slow-flow model provides good approximation of the original dynamics and the entire resonance processes as well.

In this study, we show that even though the system of coupled oscillators possesses essential (nonlinearizable) stiffness nonlinearities, analytical modeling of its dynamics at certain motion regimes can still be performed by means of the multifrequency complexification/averaging method.

Focusing first on the fundamental energy pumping mechanism, we again consider system (1) and introduce the new complex variables

$$\begin{aligned} \psi_1(t) &= \dot{v}(t) + jv(t) \equiv \varphi_1(t)\, e^{jt}, \\ \psi_2(t) &= \dot{y}(t) + jy(t) \equiv \varphi_2(t)\, e^{jt}, \end{aligned} \tag{4}$$

where $\varphi_i(t)$, $i = 1, 2$, represent slowly varying complex amplitudes and $j = (-1)^{1/2}$. By writing (4) we introduce a partition of the dynamics into slow and fast components and seek slowly modulated fast oscillations at frequency $\omega = \omega_0 = 1$. As discussed previously, fundamental energy pumping is associated with this type of motion in the neighborhood of branch $S11+$ in the frequency-energy plot of the undamped

dynamics. Expressing the system responses in terms of the new complex variables, $y = (\psi_2 - \psi_2^*)/2j$, $v = (\psi_1 - \psi_1^*)/2j$ (where $(*)$ denotes complex conjugate); substituting into (1) with $P(t) = 0$; and averaging over the fast frequency, we derive a set of approximate slow modulation equations that govern the evolutions of the complex amplitudes,

$$\begin{aligned}
&\dot{\varphi}_1 + \left(\frac{j}{2}\right)\varphi_1 + \left(\frac{\lambda}{2}\right)(\varphi_1 - \varphi_2) - \left(\frac{3jC}{8\varepsilon}\right)|\varphi_1 - \varphi_2|^2(\varphi_1 - \varphi_2) = 0,\\
&\dot{\varphi}_2 - \left(\frac{\varepsilon\lambda}{2}\right)(\varphi_1 - \varphi_2) - \left(\frac{3jC}{8}\right)|\varphi_2 - \varphi_1|^2(\varphi_2 - \varphi_1) + \left(\frac{\varepsilon\lambda}{2}\right)\varphi_2 = 0.
\end{aligned} \tag{5}$$

For the sake of simplicity, we have assumed that $\lambda_1 = \lambda_2 = \lambda$ in (1). To derive a set of real modulation equations, we express the complex amplitudes in polar form, $\varphi_i(t) = a_i(t)\, e^{j\beta_i(t)}$, $i = 1, 2$, substitute into (5), and separately set equal to zero the real and imaginary parts. We then reduce (5) to an autonomous set of equations that govern the slow evolution of the two amplitudes $a_1(t)$ and $a_2(t)$ and the phase difference $\phi(t) = \beta_2(t) - \beta_1(t)$:

$$\begin{aligned}
&\dot{a}_1 + \left(\frac{\lambda}{2}\right)a_1 - \left(\frac{\lambda}{2}\right)a_2\cos\phi - \left(\frac{3C}{8\varepsilon}\right)\left(a_1^2 + a_2^2 - 2a_1a_2\cos\phi\right)a_2\sin\phi = 0,\\
&\dot{a}_2 - \left(\frac{\varepsilon\lambda}{2}\right)a_1\cos\phi + \varepsilon\lambda a_2 + \left(\frac{3C}{8}\right)\left(a_1^2 + a_2^2 - 2a_1a_2\cos\phi\right)a_1\sin\phi = 0,\\
&\dot{\phi} + \left(\frac{\lambda}{2}\right)\left[\left(\frac{\varepsilon a_1}{a_2}\right) + \left(\frac{a_2}{a_1}\right)\right]\sin\phi - \left(\frac{1}{2}\right)\\
&+ \left(\frac{3C}{8}\right)\left(a_1^2 + a_2^2 - 2a_1a_2\cos\phi\right)\left\{\left(\frac{1}{\varepsilon}\right)\left[1 - \left(\frac{a_2}{a_1}\right)\cos\phi\right] - \left[1 - \left(\frac{a_1}{a_2}\right)\cos\phi\right]\right\} = 0.
\end{aligned} \tag{6}$$

This reduced dynamical system governs the slow-flow dynamics of fundamental energy pumping. In particular, 1:1 *resonance capture (the underlying dynamical mechanism of fundamental energy pumping) is associated with non–time-like behavior of the phase variable ϕ or, equivalently, failure of the averaging theorem in the slow-flow* (6). Indeed, when ϕ exhibits time-like, nonoscillatory behavior, one can apply the averaging theorem over ϕ and prove that the amplitudes a_1 and a_2 decay exponentially with time and that no significant energy exchanges (energy pumping) can take place. In Figure 14(a) we depict 1:1 resonance capture in the slow-flow phase plane $(\dot{\phi}, \phi)$ for system (6) with $\varepsilon = 0.05$, $\lambda = 0.01$, $C = 1$, $\omega_0 = 1$ and initial conditions $a_1(0) = 0.01$, $a_2(0) = 0.24$, $\phi(0) = 0$. The oscillatory behavior of the phase variable in the neighborhood of the in-phase limit $\phi = 0+$ indicates 1:1 resonance capture (on branch $S11+$ of the frequency-energy plot of Figure 1) and leads to energy pumping from the linear oscillator to the NES, as evidenced by the build-up of amplitude a_1 (cf. Figure 14(b)). Escape from resonance capture is associated with time-like behavior of ϕ and rapid decrease of the amplitudes a_1 and a_2 (as predicted by averaging in (6)). A comparison of the analytical approximation (4)–(6) and direct numerical simulation for the previous initial conditions confirms the accuracy of the analysis.

Considering subharmonic energy pumping, we will focus on energy pumping in the neighborhood of tongue $S13-$ (similar analysis can be applied for other orders of subharmonic resonance captures). Due to the fact that motions in the neighborhood of $S13-$ possess two main frequency components, at frequencies 1 and 1/3, we express

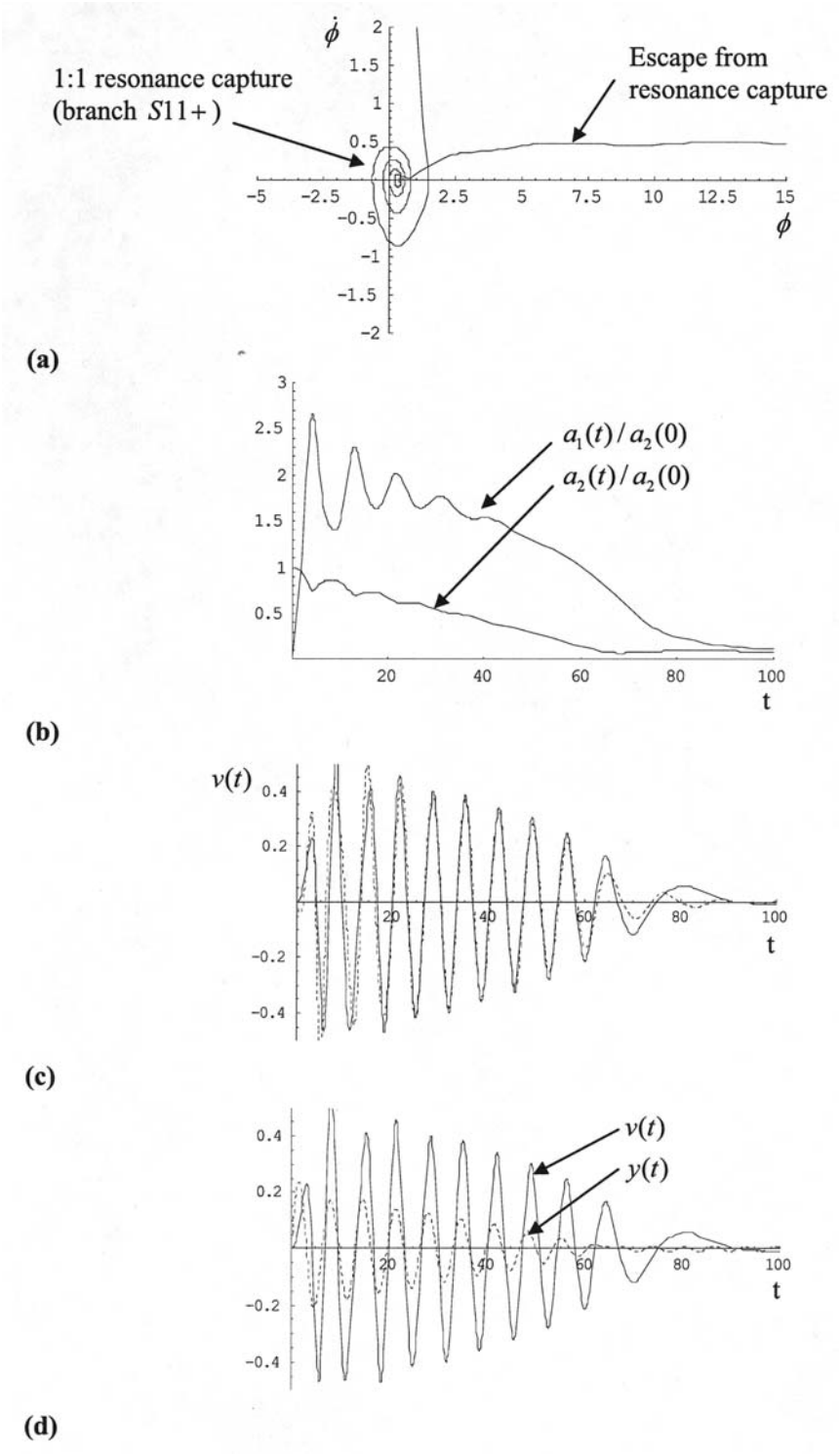

FIG. 14. *Fundamental energy pumping:* (a) 1:1 *resonance capture in the slow flow,* (b) *amplitude modulations,* (c) *comparison between analytical approximation (dashed line) and direct numerical simulation (solid line) for* $v(t)$, (d) *transient responses of the system.*

the responses of system (1) as

$$y(t) = y_1(t) + y_{1/3}(t), \qquad v(t) = v_1(t) + v_{1/3}(t), \tag{7}$$

where the indices represent the frequency of each term. As in the previous case, we introduce new complex variables,

$$\begin{aligned}
&\psi_1(t) = \dot{y}_1(t) + j\omega y_1(t) \equiv \varphi_1(t)\, e^{j\omega t}, \quad \psi_3(t) = \dot{y}_{1/3}(t) + j(\omega/3) y_{1/3}(t) \equiv \varphi_3(t)\, e^{j(\omega/3)t},\\
&\psi_2(t) = \dot{v}_1(t) + j\omega v_1(t) \equiv \varphi_2(t)\, e^{j\omega t}, \quad \psi_4(t) = \dot{v}_{1/3}(t) + j(\omega/3) v_{1/3}(t) \equiv \varphi_4(t)\, e^{j(\omega/3)t},
\end{aligned} \tag{8}$$

where $\varphi_i(t)$ represent slowly varying modulations of fast oscillations of frequencies 1 or 1/3. Expressing the system responses in terms of the new complex variables,

$$y = \frac{\psi_1 - \psi_1^*}{2j\omega} + \frac{3\,(\psi_3 - \psi_3^*)}{2j\omega}, \qquad v = \frac{\psi_2 - \psi_2^*}{2j\omega} + \frac{3\,(\psi_4 - \psi_4^*)}{2j\omega}, \tag{9}$$

substituting into (1) with $P(t) = 0$, and averaging over each of the two fast frequencies, we derive the slow modulation equations that govern the evolutions of the complex amplitudes,

$$\begin{aligned}
&\dot{\varphi}_1 + \left(\frac{j\omega}{2} - \frac{j}{2\omega}\right)\varphi_1 + \left(\frac{\varepsilon\lambda}{2}\right)(2\varphi_1 - \varphi_2) + \left(\frac{jC}{8\omega^3}\right)\Big\{3\Big[9\varphi_3^3 - 27\varphi_3^2\varphi_4 - 9\varphi_4^3\\
&\quad - (\varphi_1 - \varphi_2)\,|\varphi_1 - \varphi_2|^2 + 27\varphi_3\varphi_4^2 - 18\,(\varphi_1 - \varphi_2)\,|\varphi_3 - \varphi_4|^2\Big]\Big\} = 0,\\
&\dot{\varphi}_3 + \left(\frac{j\omega}{6} - \frac{3j}{2\omega}\right)\varphi_3 + \left(\frac{\varepsilon\lambda}{2}\right)(2\varphi_3 - \varphi_4)\\
&\quad + \left(\frac{jC}{8\omega^3}\right)\Big\{-9\Big[\varphi_1\left(2\,(\varphi_3 - \varphi_4)\,(\varphi_1^* - \varphi_2) - 3\,(\varphi_3^* - \varphi_4^*)^2\right)\\
&\quad + \varphi_2\left(2\,(\varphi_4 - \varphi_3)\,(\varphi_1^* - \varphi_2) + 3\,(\varphi_3^* - \varphi_4^*)^2\right) + 9\,(\varphi_3 - \varphi_4)\,|\varphi_3 - \varphi_4|^2\Big]\Big\} = 0,\\
&\dot{\varphi}_2 + \left(\frac{j\omega}{2}\right)\varphi_2 + \left(\frac{\lambda}{2}\right)(\varphi_2 - \varphi_1) - \left(\frac{jC}{\varepsilon 8\omega^3}\right)\Big\{3\Big[9\varphi_3^3 - 27\varphi_3^2\varphi_4 - 9\varphi_4^3\\
&\quad - (\varphi_1 - \varphi_2)\,|\varphi_1 - \varphi_2|^2 + 27\varphi_3\varphi_4^2 - 18\,(\varphi_1 - \varphi_2)\,|\varphi_3 - \varphi_4|^2\Big]\Big\} = 0,\\
&\dot{\varphi}_4 + \left(\frac{j\omega}{6}\right)\varphi_4 + \left(\frac{\lambda}{2}\right)(\varphi_4 - \varphi_3)\\
&\quad - \left(\frac{jC}{\varepsilon 8\omega^3}\right)\Big\{-9\Big[\varphi_1\left(2\,(\varphi_3 - \varphi_4)\,(\varphi_1^* - \varphi_2) - 3\,(\varphi_3^* - \varphi_4^*)^2\right)\\
&\quad + \varphi_2\left(2\,(\varphi_4 - \varphi_3)\,(\varphi_1^* - \varphi_2) + 3\,(\varphi_3^* - \varphi_4^*)^2\right) + 9\,(\varphi_3 - \varphi_4)\,|\varphi_3 - \varphi_4|^2\Big]\Big\} = 0,
\end{aligned} \tag{10}$$

where again it was assumed that $\lambda_1 = \lambda_2 = \lambda$ in (1). To derive a set of real modulation equations, we express the complex amplitudes in polar forms $\varphi_i(t) = a_i(t)\, e^{j\beta_i(t)}$ and derive an autonomous set of seven slow-flow modulation equations that govern the amplitudes $a_i = |\varphi_i|$, $i = 1, \ldots, 4$, and the phase differences $\phi_{12} = \beta_1 - \beta_2$, $\phi_{13} = \beta_1 - 3\beta_3$, and $\phi_{14} = \beta_1 - 3\beta_4$.

The equations of the autonomous slow flow will not be reproduced here, but it suffices to state that they are of the form

$$
\begin{aligned}
&\dot{a}_1 + \left(\frac{\varepsilon\lambda}{2}\right)(2a_1 - a_2) + g_1(a,\phi) = 0,\\
&\dot{a}_3 + \left(\frac{\varepsilon\lambda}{2}\right)(2a_3 - a_4) + g_3(a,\phi) = 0,\\
&\dot{a}_2 + \left(\frac{\lambda}{2}\right)(a_2 - a_1) + \frac{g_2(a,\phi)}{\varepsilon} = 0,\\
&\dot{a}_4 + \left(\frac{\lambda}{2}\right)(a_4 - a_3) + \frac{g_4(a,\phi)}{\varepsilon} = 0,\\
&\dot{\phi}_{12} + f_{12}(a) + g_{12}(a,\phi;\varepsilon) = 0,\\
&\dot{\phi}_{13} + f_{13}(a) + g_{13}(a,\phi) = 0,\\
&\dot{\phi}_{14} + f_{14}(a) + g_{14}(a,\phi;\varepsilon) = 0,
\end{aligned}
\tag{11}
$$

where the functions g_i and g_{ij} are 2π-periodic in terms of the phase angles $\phi = (\phi_{12}\ \phi_{13}\ \phi_{14})^T$ and by a we denote the (4×1) vector of the amplitudes a_i. In this case (as for the fundamental energy pumping mechanism), strong energy transfer between the linear and nonlinear oscillators can occur only when a subset of phase angles ϕ_{ij} does not exhibit time-like behavior; that is, when some phase angles possess oscillatory (nonmonotonic) behavior with respect to time. This can be seen from the structure of the slow flow (11) where, if the phase angles exhibit time-like behavior and the functions g_i are small, averaging over these phase angles can be performed to show that the amplitudes a_i decrease monotonically with time; in that case no significant energy exchanges between the linear and nonlinear components of the system can take place. It follows that *subharmonic energy pumping is associated with non–time-like behavior of (at least) a subset of the slow phase angles* ϕ_{ij} *in* (11).

In Figure 15 we present the results of the numerical integration of the slow-flow (10)–(11) for the system with parameters $\varepsilon = 0.05$, $\lambda = 0.03$, $C = 1$, $\omega_0 = 1$. The motion is initiated on branch $S13-$ with initial conditions $v(0) = y(0) = 0$ and $\dot{v}(0) = 0.01499$, $\dot{y}(0) = -0.059443$ (it corresponds exactly to the simulation of Figure 5). The corresponding initial conditions and the value of the frequency ω of the reduced slow-flow model were computed by minimizing the difference between the analytical and numerical responses of the system in the interval $t \in [0, 100]$: $\varphi_1(0) = -0.0577$, $\varphi_2(0) = 0.0016$, $\varphi_3(0) = -0.0017$, $\varphi_4(0) = 0.0134$, and $\omega = 1.0073$. This result indicates that, initially, nearly all energy is stored in the fundamental frequency component of the linear oscillator, with the remainder confined to the subharmonic frequency component of the NES. In Figures 15(a)–(b) we depict the temporal evolution of the amplitudes a_i, from which we conclude that subharmonic energy pumping in the system is mainly realized through energy transfer from the (fundamental) component at frequency ω of the linear oscillator, to the (subharmonic) component at frequency $\omega/3$ of the NES (as judged from the build-up of the amplitude a_3 and the diminishing of a_1). A smaller amount of energy is transferred from the fundamental frequency component of the linear oscillator to the corresponding fundamental component of the NES (as judged by the evolution of the amplitude a_2).

These conclusions are supported by the plots of Figures 15(c)–(e), where the temporal evolutions of the phase differences $\phi_{12} = \beta_1 - \beta_2$, $\phi_{13} = \beta_1 - 3\beta_3$, and $\phi_{14} = \beta_1 - 3\beta_4$ are shown. Absence of strong energy exchange between the funda-

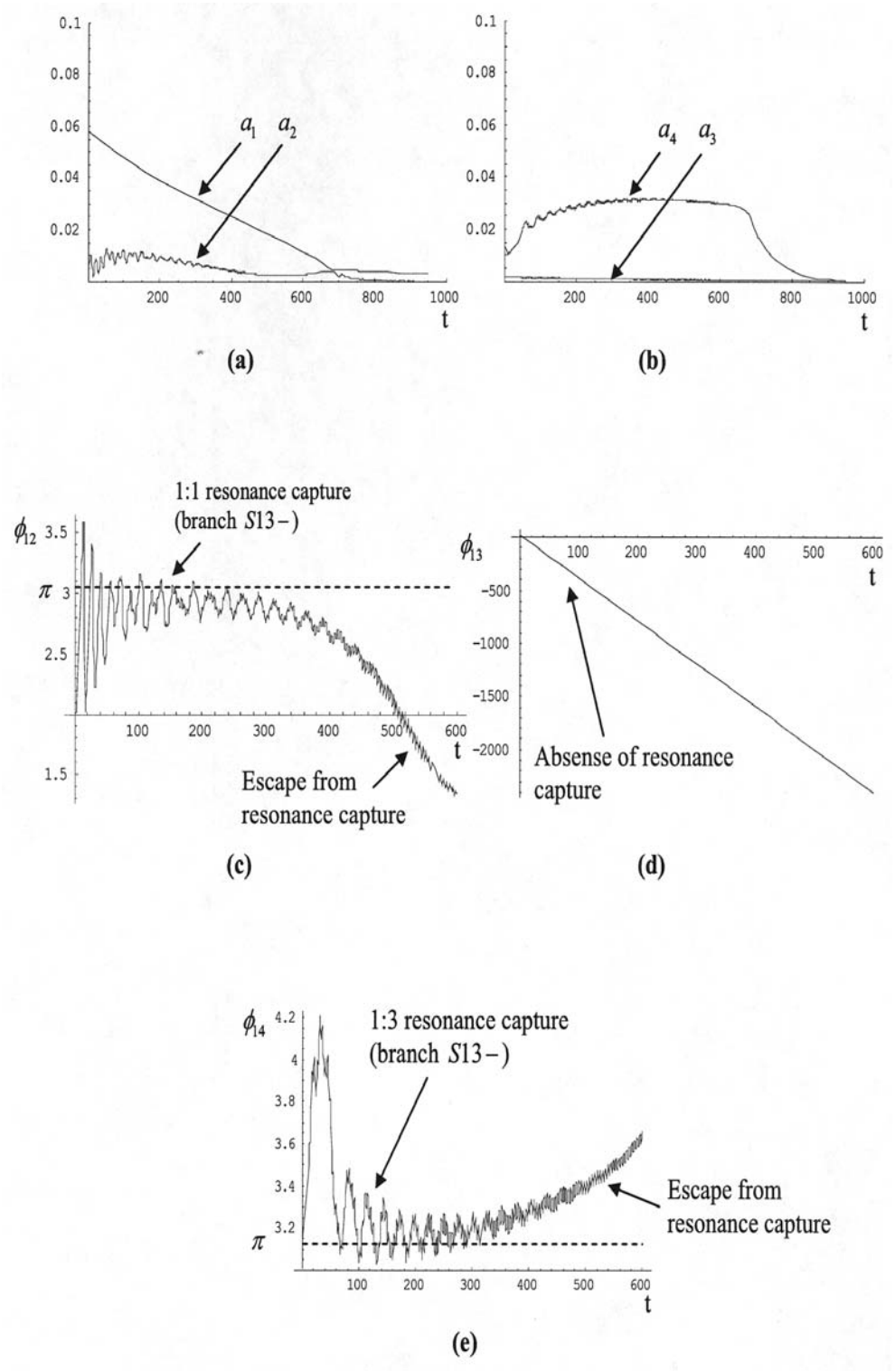

FIG. 15. *Subharmonic energy pumping:* (a), (b) *amplitude modulations;* (c), (d), (e) *phase modulations.*

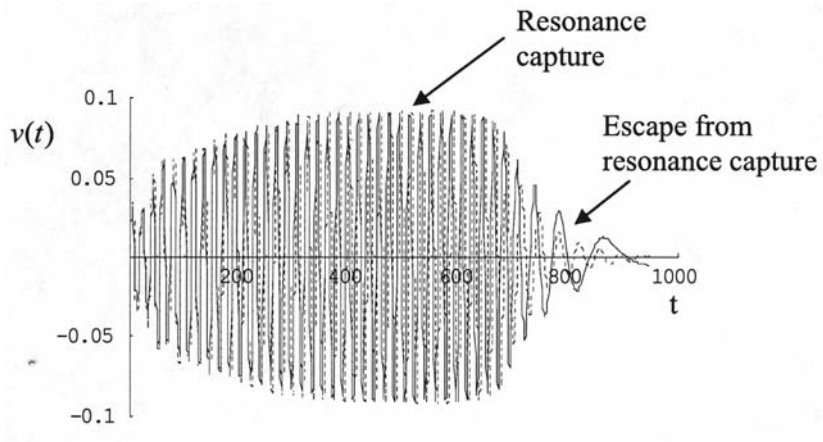

FIG. 16. *Transient response of NES for* 1:3 *subharmonic energy pumping: comparison between analytical approximation (dashed line) and direct numerical simulation (solid line).*

mental and subharmonic frequency components of the linear oscillator is associated with the time-like behavior of the phase difference ϕ_{13}, whereas energy pumping from the fundamental component of the linear oscillator to the two frequency components of the NES is associated with oscillatory early-time behavior of the phase differences ϕ_{12} and ϕ_{14}. Oscillatory responses of ϕ_{12} and ϕ_{14} correspond to 1:1 and 1:3 resonance captures, respectively, between the corresponding frequency components of the linear oscillator and the NES; as time increases, time-like responses of the phase variables are associated with escapes from the corresponding regimes of resonance capture. In addition, we note that the oscillations of the angles ϕ_{12} and ϕ_{14} take place in the neighborhood of π, which confirms that, in this particular example, subharmonic energy pumping is activated by the excitation of an antiphase branch of periodic solutions (such as $S13-$). The analytical results are in full agreement with the wavelet transforms depicted in Figures 5(c)–(d), where the response of the linear oscillator possesses a strong frequency component at the fundamental frequency $\omega_0 = 1$, whereas the NES oscillates mainly at frequency $\omega_0/3$.

The accuracy of the analytical model (10)–(11) in capturing the dynamics of subharmonic energy pumping is confirmed by the plot depicted in Figure 16, where the analytical response of the NES is found to be in satisfactory agreement with the numerical response obtained by the direct simulation of (1). It is interesting to note that the reduced analytical model is capable of accurately modeling the strongly nonlinear, damped, transient response of the NES in the resonance capture region. The analytical model fails, however, during the escape from resonance capture since the ansatz (7)–(8) is not valid in that regime of the motion. Indeed, after escape from resonance capture, the motion approximately evolves along the backbone curve of the frequency-energy plot; eventually $S15$ is reached, the motion of which cannot be described by the ansatz (7)–(8), thereby leading to the failure of the analytical model.

The results presented so far provide a measure of the complicated dynamics encountered in the two-DOF system under consideration. It is logical to assume that by increasing the degrees of freedom of the system the dynamics will be even more complex. That this is indeed the case is evidenced by the numerical simulations presented in the next section, where resonance capture cascades are reported in multi-degree-

of-freedom (MDOF) linear systems with essentially nonlinear end attachments. By resonance capture cascades we denote complicated sudden transitions between different branches of solutions (modes), which are accompanied by sudden changes in the frequency content of the system responses. As shown in previous works (Vakakis et al. (2003)), such multifrequency transitions can drastically enhance energy pumping from the linear system to the essentially nonlinear attachment.

5. Increasing the DOF of the linear system: Resonance capture cascades. To provide an indication of the complex multifrequency transitions that can take place in coupled oscillators with essentially nonlinear local attachments, we now increase the number of DOF of the linear subsystem to two and examine the system

$$\begin{gathered} \ddot{y}_2 + \omega_0^2 y_2 + \lambda_2 \dot{y}_2 + d(y_2 - y_1) = 0, \\ \ddot{y}_1 + \omega_0^2 y_1 + \lambda_1 \dot{y}_1 + \lambda_3(\dot{y}_1 - \dot{v}) + d(y_1 - y_2) + C(y_1 - v)^3 = 0, \\ \varepsilon \ddot{v} + \lambda_3(\dot{v} - \dot{y}_1) + C(v - y_1)^3 = 0. \end{gathered} \tag{12}$$

The system parameters are chosen as $\omega_0^2 = 136.9$, $\lambda_1 = \lambda_2 = 0.155$, $\lambda_3 = 0.544$, $d = 1.2 \times 10^3$, $\varepsilon = 1.8$, and $C = 1.63 \times 10^7$, with linear natural frequencies $\omega_1 = 11.68$ and $\omega_2 = 50.14$.

In Figure 17(a) we depict the relative response $v(t) - y_1(t)$ of the system for initial displacements $y_1(0) = 0.01$, $y_2(0) = v(0) = -0.01$ and zero initial velocities. The multifrequency content of the transient response is evident and is quantified in Figure 17(b), where the instantaneous frequency of the time series is computed by applying the numerical Hilbert transform (Huang et al. (1998)).

As energy decreases due to damping dissipation, a series of eight *resonance capture cascades* is observed, i.e., of transient resonances of the NES with a number of nonlinear modes of the system. The complexity of the nonlinear dynamics of the system is evidenced by the fact that of these eight captures only two (labeled IV and VII in Figure 17(b)) involve the linearized in-phase and out-of-phase modes of the linear oscillator, with the remaining involving essentially nonlinear interactions of the NES with different low- and high-frequency nonlinear modes of the system. During each resonance capture the NES passively absorbs energy from the nonlinear mode involved, before escape from resonance capture occurs and the NES transiently resonates with the next mode in the series. In essence, *the NES acts as a passive, broadband boundary controller*, absorbing, confining, and eliminating vibration energy from the linear oscillator. Similar types of resonance capture cascades were reported in previous works where grounded NESs, weakly coupled to the linear structure, were examined (Vakakis et al. (2003)). The capacity of the NES to resonantly interact with linear and nonlinear modes in different frequency ranges is due to its essential nonlinearity (i.e., the absence of a linear term in the nonlinear stiffness characteristic), which precludes any preferential resonant frequency.

Finally, we note that the complex nonlinear transitions between modes depicted in Figure 17 can be interpreted and understood by studying the topology and bifurcations of periodic orbits of the corresponding undamped system. As shown in previous sections, the weakly damped, forced dynamics is expected to depend on the periodic dynamics of the underlying undamped system.

6. Concluding remarks. Even though the systems considered in this work possess rather simple configurations and small numbers of DOF, they exhibit interesting passive energy transfer properties. Indeed, under rather general conditions, it is possible to transfer passively, irreversibly, and robustly a significant portion of the energy

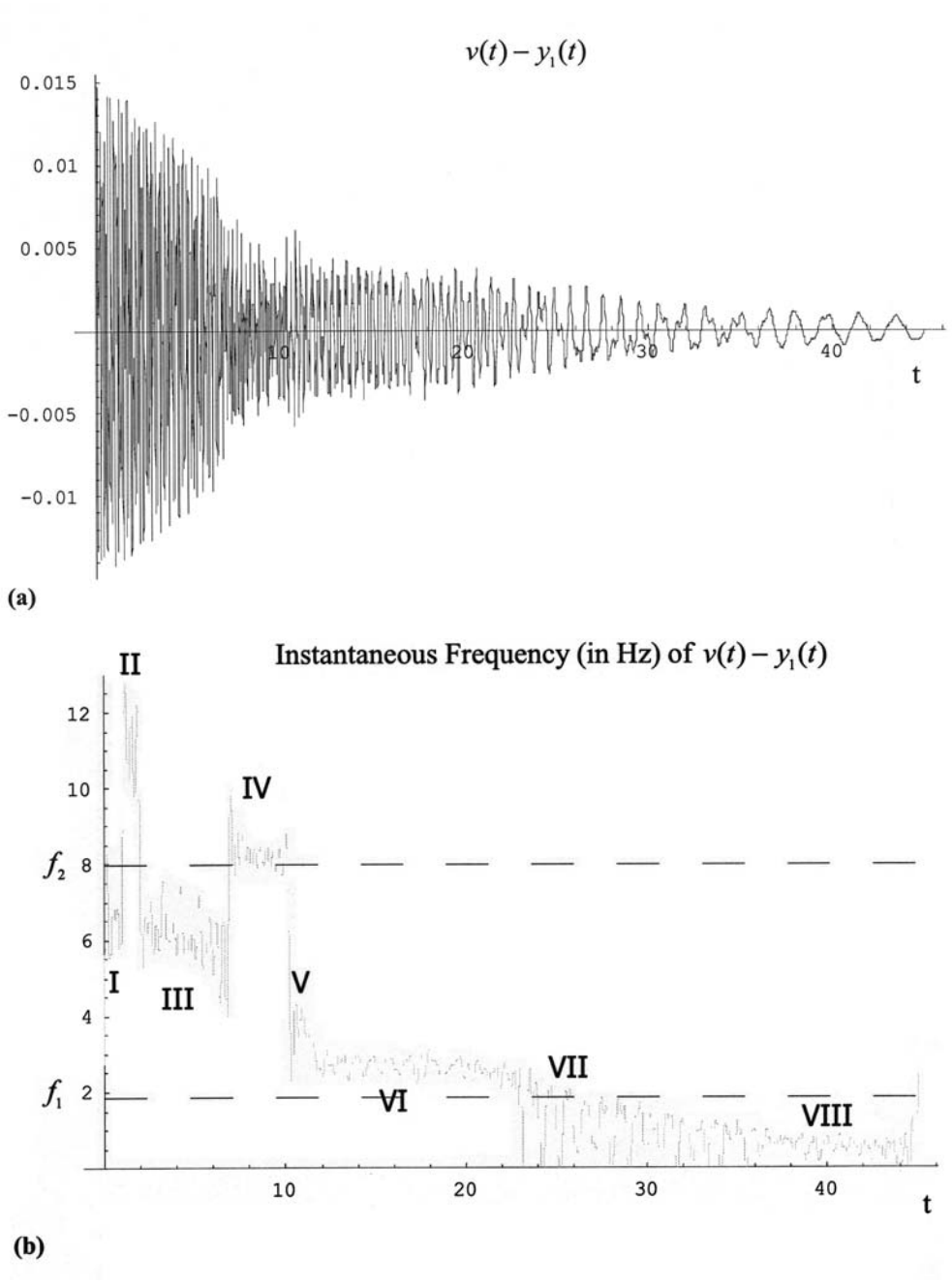

FIG. 17. *Resonance capture cascades in the* 2*-DOF system with nonlinear end attachment:* (a) *relative transient response* $v(t) - y_1(t)$*;* (b) *instantaneous frequency (resonance captures indicated).*

of the linear oscillator to the nonlinear attachment; confine it; and passively dissipate it locally without "radiating back" the transferred energy to the primary system. Moreover, this nonlinear energy pumping occurs over low- as well as high-frequency ranges, and involves broadband disturbances. This last feature clearly distinguishes

the present configuration from previous classical vibration absorber designs, where energy absorption was limited to narrowband disturbances, and the absorbers were effective only in the vicinity of a single frequency.

Three mechanisms for energy pumping were discussed in this work. Two of them rely on resonance capture of the damped dynamics on either fundamental or subharmonic resonant manifolds in phase space. Viewed from a different perspective, in these cases irreversible energy transfer from the linear oscillator to the nonlinear attachment takes place when the dynamics is restricted to a damped nonlinear normal mode invariant manifold, whose mode shape becomes strongly localized to the nonlinear attachment as the energy deceases due to damping dissipation. A third mechanism relies on nonlinear beats to initiate (but not cause) strong energy pumping; these beats act as "bridging orbits" (or "catalysts") for facilitating energy transfer by activating either one of the previously mentioned mechanisms. It is interesting that all these phenomena occur despite the lightness of the nonlinear attachment compared to the linear oscillator and the complete absence of any active (energy source) element in the system.

The considered nonlinear attachment holds promise as an efficient, robust, and modular passive absorbing device for eliminating undesired broadband disturbances of small- or large-scale structures. As such it can find application in diverse problems in engineering and physics, including vibration and shock isolation of machines and structures, seismic mitigation, packaging, and instability (such as limit cycle oscillation or flutter) suppression.

REFERENCES

S. Aubry, S. Kopidakis, A. M. Morgante, and G. P. Tsironis (2001), *Analytic conditions for targeted energy transfer between nonlinear oscillators or discrete breathers*, Phys. B, 296, pp. 222–236.

C. W. Cai, H. C. Chan, and Y. K. Cheung (2000), *Localized modes in a two-degree-coupled periodic system with a nonlinear disordered subsystem*, Chaos Solitons Fractals, 11, pp. 1481–1492.

M. F. Golnaraghi (1991), *Vibration suppression of flexible structures using internal resonance*, Mech. Res. Comm., 18, pp. 135–143.

N. E. Huang, Z. Shen, S. R. Long, M. C. Wu, H. H. Shih, Q. Zheng, N.-C. Yen, C. C. Tung, and H. H. Liu (1998), *The empirical mode decomposition and the Hilbert spectrum for nonlinear and non-stationary time series analysis*, R. Soc. Lond. Proc. Ser. A Math. Phys. Eng. Sci., 454, pp. 903–995.

K. R. Khusnutdinova and D. E. Pelinovsky (2003), *On the exchange of energy in coupled Klein–Gordon oscillators*, Wave Motion, 38, pp. 1–10.

G. Kopidakis, S. Aubry, and G. P. Tsironis (2001), *Targeted energy transfer through discrete breathers in nonlinear systems*, Phys. Rev. Lett., 87, paper 165501-1.

Y. S. Lee, G. Kerschen, A. F. Vakakis, P. Panagopoulos, L. A. Bergman, and D. M. McFarland (2005), *Complicated dynamics of a linear oscillator with an essentially nonlinear local attachment*, Phys. D, 204, pp. 41–69.

P. Malatkar and A. H. Nayfeh (2003), *On the transfer of energy between widely spaced modes in structures*, Nonlinear Dynam., 31, pp. 225–242.

L. I. Manevitch (1999), *Complex representation of dynamics of coupled oscillators*, in Mathematical Models of Nonlinear Excitations, Transfer Dynamics and Control in Condensed Systems, Kluwer Academic Publishers/Plenum, New York, pp. 269–300.

P. Maniadis, G. Kopidakis, and S. Aubry (2004), *Classical and quantum targeted energy transfer between nonlinear oscillators*, Phys. D, 188, pp. 153–177.

A. M. Morgante, M. Johansson, S. Aubry, and G. Kopidakis (2002), *Breather-phonon resonances in finite-size lattices: "Phantom breathers,"* J. Phys. A, 35, pp. 4999–5021.

A. I. Neishtadt (1997), *Scattering by resonances*, Celest. Mech. Dynam. Astronom., 65, pp. 1–20.

A. I. Neishtadt (1999), *On adiabatic invariance in two-frequency systems*, in Hamiltonian Systems with Three or More Degrees of Freedom, NATO Adv. Sci. Inst. Ser. C Math. Phys. Sci. 533, Kluwer Academic Publishers, Norwell, MA, pp. 193–213.

P. Salemi, M. F. Golnaraghi, and G. R. Heppler (1997), *Active control of forced and unforced structural vibration*, J. Sound Vibration, 208, pp. 15–32.

D. L. Vainchtein, E. V. Rovinsky, L. M. Zelenyi, and A. I. Neishtadt (2004), *Resonances and particle stochastization in nonhomogeneous electromagnetic fields*, J. Nonlinear Sci., 14, pp. 173–205.

A. F. Vakakis and O. Gendelman (2001), *Energy pumping in nonlinear mechanical oscillators* II: *Resonance capture*, J. Appl. Mech., 68, pp. 42–48.

A. F. Vakakis, L. I. Manevitch, Yu. V. Mikhlin, V. N. Pilipchuk, and A. A. Zevin (1996), *Normal Modes and Localization in Nonlinear Systems*, Wiley Interscience, New York.

A. F. Vakakis, L. I. Manevitch, O. Gendelman, and L. A. Bergman (2003), *Dynamics of linear discrete systems connected to local essentially nonlinear attachments*, J. Sound Vibration, 264, pp. 559–577.

S. J. Zhu, Y. F. Zheng, and Y. M. Fu (2004), *Analysis of nonlinear dynamics of a two-degree-of-freedom vibration system with nonlinear damping and nonlinear spring*, J. Sound Vibration, 271, pp. 15–24.